JACS
JOURNAL OF THE AMERICAN CHEMICAL SOCIETY

Article

pubs.acs.org/JACS

Supramolecular Organization and Magnetic Properties of Mesogen-Hybridized Mixed-Valent Manganese Single Molecule Magnets $[Mn^{III}_8Mn^{IV}_4O_{12}(L_{x,y,z\text{-CB}})_{16}(H_2O)_4]$

Emmanuel Terazzi,[†] Guillaume Rogez, Jean-Louis Gallani, and Bertrand Donnio*

Institut de Physique et Chimie des Matériaux de Strasbourg (IPCMS), UMR 7504, CNRS-Université de Strasbourg, 23 rue du Loess, BP43, 67034, Strasbourg cedex 2, France

Ⓢ *Supporting Information*

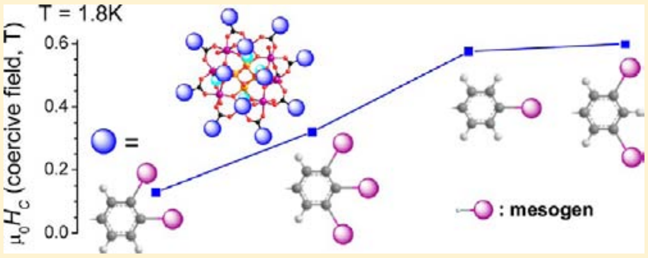

ABSTRACT: Single molecule magnets (SMM) may be considered for the construction of future integrated nano-devices, provided however that some degree of ordering is imparted to these molecules (surfaces nanostructuration). Combining such nanoobjects with liquid-crystalline orderings to control their assembly and to potentially address them individually therefore appears as one promising strategy. Four mesomorphic, mixed-valent $[Mn^{III}_8Mn^{IV}_4O_{12}(L_{x,y,z\text{-CB}})_{16}(H_2O)_4]$ SMM, differing in the number of liquid-crystalline promoters, ($L_{x,y,z\text{-CB}}$), were synthesized, and their self-organizing and magnetic properties were investigated. The influence of the peripheral modifications, and precisely how supramolecular ordering and magnetic properties may be affected by the evolution of the proto-mesogenic cyanobiphenyl-based ligands substitution pattern, was explored. Small-angle X-ray scattering studies revealed that all of the hybridized clusters self-organize into room-temperature bilayer smectic phases, mandated by the specific mesogenic functionalization and that the polymetallic cores are further organized according to a short-range pseudo-2D lattice with hexagonal and/or square symmetry. All mesomorphous hybridized dodecamanganese complexes still behave as SMM: they exhibit blocking of the magnetization at about 2.6 K as evidenced by the occurrence of frequency-dependent out-of-phase ac susceptibility signals as well as an opening of the hysteresis cycle with coercive fields varying between 0.13 and 0.6 T, depending on the surface ligands topology. Comparison of the magnetic properties within this series reveals intricate correlations between the structural features of the mesomorphous molecule magnet (i.e., symmetry of the ligands substitution patterns, molecular conformation, average intercluster distances, and respective inclination) with respect to the relative proportion of slow- and fast-relaxing species and the absolute values of the coercive fields.

■ INTRODUCTION

Usually, for traditional materials, ferromagnetism is a collective phenomenon and is the fact of an enormous number of atoms, organized in such a way that their electrons' magnetic moments interact cooperatively to form a permanent magnet. The discovery that some peculiar molecules, for example, the so-called single molecule magnets (SMM), could also function individually as single "nano"-magnets by retaining a magnetization at the molecular level revived intense research activity in the field of molecular magnetism.[1] Indeed, below a certain temperature, T_B, known as the blocking temperature, and in the absence of a magnetic field, the magnetic moment of a SMM stops fluctuating and becomes stable, without the need for domains, walls, and long-range ordering of the magnetic moments (no exchange interaction). Independent of their academic interest, SMM, among other nanomagnetic materials,[2] may be considered as ideal candidates to transcend the superparamagnetic frontier, which currently limits the technology of magnetic information storage to densities of the order of 400 Gb/in.^{2} (e.g., gigabit per square inch).[3] They moreover are envisioned as building blocks (qubits) for implementing quantum algorithms in computers because of their intrinsic quantum nature.[3,4] High-density information storage, molecular spintronics, and processing at the molecular level could indeed be the technological jump leading to the next generation of computers. Still, a good number of progresses and breakthroughs remain to be achieved before any of these dreams come true: rational design and organization of SMM on a surface remain elusive,[5] addressing a single molecule is a technological challenge,[6] and all of the SMM discovered until now lose their properties above 6 K at best.[7]

SMM usually possess a high-spin ground state brought by 3d (and also 4d and/or 4f)[1,7] metal ions: the highest spin value observed so far is S = 51/2 for a SMM Mn25 complex[8] (the highest spin reported for a non-SMM compound is S = 83/2 for a Mn19 cluster[9]). The first and now very famous SMM cluster is the so-called mixed-valent "manganese 12" (Mn12) with the general formula $[Mn^{III}_8Mn^{IV}_4O_{12}(CH_3CO_2)_{16}(H_2O)_4]$ (Figure 1), $[Mn_{12}(OAc)_{16}]$ for short, serendipitously synthe-

Received: November 14, 2012
Published: January 22, 2013

dx.doi.org/10.1021/ja311190a | *J. Am. Chem. Soc.* 2013, 135, 2708−2722

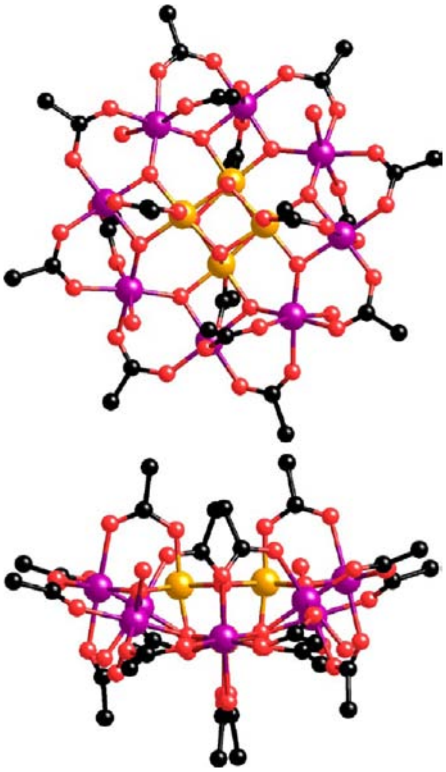

Figure 1. Crystallographic structure of $[Mn_{12}(OAc)_{16}]$ complex along the crystal *c*-axis (top) and *b*-axis (bottom). Color scheme: Mn^{IV}, yellow; Mn^{III}, purple; O, red; C, black.

sized by Lis in 1980,[10] but whose magnetic bistability was demonstrated only a decade later by Gatteschi et al.[11] This prototypical molecular nanomagnet[12] has one of the highest blocking temperature ($T_B \approx 3.7$ K, for a characteristic relaxation time $\tau = 100$ s, see below), its spin ground state reaches a rather high value ($S = 10$), and its coercive field also is quite impressive ($\mu_0 H_c \approx 1$ T at 2 K). This mixed-valence polyoxometallate core contains 12 manganese ions, and its structure consists of a roughly planar disk made up of a central $Mn^{IV}_4O_4$ cubane moiety (Mn^{IV}, $S = 3/2$) surrounded by a ring of eight Mn^{III} ions ($S = 2$), connected to the cube by eight μ_3-O^{2-} ions and four κ^2-μ_2-acetate groups perpendicular to the plane of the disk (two on each side, Figure 1). The peripheral Mn^{III} centers are further connected to each other by eight equatorial and four axial κ^2-μ_2-acetate groups; consequently, the Mn^{III} ions of the outer ring are alternatively doubly bridged to one and singly bridged to two Mn^{IV} ions (referred to as Mn^{III} of type I or II, respectively). Generally, the magnetic couplings between the core metal ions are almost never entirely ferromagnetic: some ions are ferromagnetically coupled, some antiferromagnetically, and the total spin of the cluster therefore rarely is the bare sum of all of the individual spins of the ions. In $[Mn_{12}(OAc)_{16}]$, the outer Mn^{III} ions are coupled ferromagnetically, and so are the inner Mn^{IV} ions, but the two subsets are coupled antiferromagnetically.[13]

As just a high spin is not enough, there must also be some Ising magnetic anisotropy (easy magnetic axis), i.e., a negative zero-field splitting parameter, *D*, which creates an energy barrier, U_{eff}, to the thermal relaxation of the magnetization.[14] This barrier is around 61 K for $[Mn_{12}(OAc)_{16}]$,[15] while the highest value reported so far for a SMM is 86.4 K.[16] In $[Mn_{12}(OAc)_{16}]$, most of the magnetic anisotropy of the ground state stems from the magnetic anisotropy of the eight outermost Mn^{III} ions. The coordination around each Mn^{III} ion is actually not a regular octahedral, but is Jahn−Teller (JT) distorted, as two bonds are longer than the other four (JT elongation).[17−19] These crystal-field distortions together with a spin−orbit interaction result in a zero-field interaction at each Mn^{III} ion; hence, vectorial projection of single-ion anisotropies on to the ground state gives rise to the easy axis anisotropy.

Numerous, and versatile, homo- and heterometallic molecular structures (based on 3d−5d and/or 4f metal ions with all sorts of peripheral ligands),[1,7,12] from single metal-ion to high-nuclearity complexes (e.g., Mn84[20]), have been synthesized, as well as various approaches (e.g., ligand surface-modification,[21] applying pressure[22,23]) have been undertaken, which were directly aiming at improving one or several of these parameters (S, D, U_{eff}). To the chemist's despair, however, the original compound often remains the best compromise. Even though sometimes successful, the random testing of new structures is not the most efficient way. The traditional approach therefore usually relies on trying to modify one parameter at a time and look for the subsequent evolution of the physical properties. Unfortunately, the intramolecular magnetic couplings are exquisitely sensitive to bonds' lengths and angles, making the accurate tweaking somehow hazardous: the nature of the magnetic coupling between metal centers, and particularly within Mn-based cores, highly depends on the mechanical influence of peripheral ligands, because the magnetic coupling are often mediated by O or N atoms and sensitive to bond angles and interatomic distances (Mn12,[24,25] Mn6[7,16,26]). For $[Mn_{12}(OAc)_{16}]$, the correlation between magnetic properties and molecular geometry was confirmed because changes were essentially ascribed to either variation of the angle between the JT axis and the S_4 molecular axis or enhancement of JT isomerism. The influence of the torsion of the JT axis on the magnetic anisotropy is also theoretically expected.[27,28] All of these results prove that the deliberate distortions and deformations that can be inflicted to the molecular structure without its destruction can indeed influence the final magnetic properties, but have a limited action range, and therefore this strategy will never enable the rise of the energy barrier up to an arbitrarily high value. Applying an anisotropic pressure by chemical means, that is, through the use of appropriate anisotropic ligands, is a priori more interesting, although such a synthetic control also appears as a difficult challenge.

Liquid crystals (LC) are outstanding examples of soft, molecular self-assemblies that exquisitely combine order and fluidity, within components self-organizing into a wide diversity of mobile and long-range ordered, periodic structures.[29,30] Furthermore, LC assemblies can easily form thin films, which are intrinsically defect-tolerant because positioning errors are corrected automatically during the process of self-assembly. Their dynamic nature, function-integration, and stimuli-responsiveness abilities further render them more inevitable for applications in modern technologies and particularly in organic electronics.[31] The formation of ordered yet fluid LC mesophases may thus be sought as a first step in the route to controlling the assembly of single molecule magnets into low-dimensional supramolecular orderings for their ultimate incorporation within functional macroscopic devices (moleconic-, spintronic-, magneto-optic-, magneto-electric-based systems).[3,5,6] We have already reported how Mn12 clusters could be endowed with mesomorphic character, without losing their original low-temperature magnetic properties.[32] The

Scheme 1. Schematic Representation of the Solvent-Mediated Ligand-Exchange Reaction and Chemical Structures of the Cyanobiphenyl-Substituted Benzoic Acid Derivatives Used as Ligands ($HL_{x,y,z}$-CB)

$$[Mn_{12}O_{12}(CH_3CO_2)_{16}(H_2O)_4] + 16HL_{x,y,z\text{-CB}} \xrightleftharpoons{CH_2Cl_2/Toluene} [Mn_{12}O_{12}(L_{x,y,z\text{-}CB})_{16}(H_2O)_4] + 16CH_3CO_2H$$

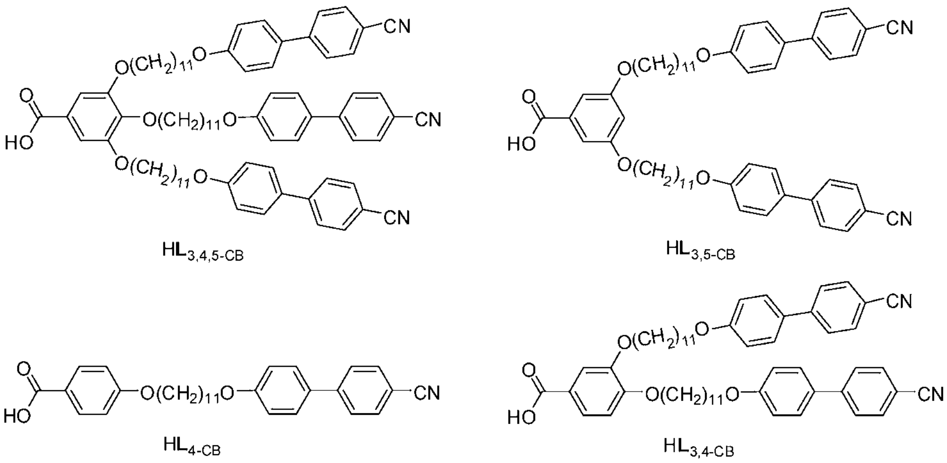

induction of thermotropic smectic or cubic mesophases was achieved through chemical exchange reaction of the acetates with protomesogenic gallic acid-based derivatives. We therefore come closer to the aforementioned goal of 3D-organizing functional entities at the nanoscale. Addressing nano-objects in 3D is quite challenging, but first XMCD results did cast doubts about the stability of the magnetic behavior of SMM on surfaces.[33] Shortly after, nevertheless, it was shown that the magnetism in itself was not altered, but that the observed behavior most probably was the result of an unforeseen photomagnetic effect.[34,35] Interestingly, this unexpected photosensitivity of LC Mn12 derivatives could allow addressing the magnetic state of the molecule using a combination of light and magnetic field and therefore facilitate the use of these SMM in a molecular memory.

We shall describe our attempt for controlling the supramolecular mesomorphic organization and the magnetic parameters of a complete set of liquid-crystalline Mn12 single molecule magnets containing cyanobiphenyl peripheral groups. The design, synthesis, and functionalization by ligand-exchange method, and the characterization of their self-organization into LC smectic phases, and their peculiar SMM properties will be described. The present study aimed at understanding and rationalizing the influences of specific structural variations introduced in the molecular system, the evolution of the substitution pattern of the ligands, their consequences on the supramolecular organizations, and the impact of space-structuring on the magnetic properties. In particular, we shall show how the use of anisotropic pro-mesogenic ligands can provide a means for finely tuning the molecular geometry and the magnetic properties without fundamental alteration.

■ RESULTS

The strategy developed to endow the archetypical Mn12 SMM cluster with LC properties has been inspired and adapted from a previously described methodology used to successfully force mesomorphism in hexakis(methano) C_{60}-containing compounds.[36,37] The idea consists of limiting the unfavorable effects of the bulky Mn12-based metal-coordination polyhedron spatial expansion by creating a fluid and deformable (e.g., adaptable) interface all around the "anti" mesogenic polymetallic core: the organic sheath, made of polypedal protomesogenic ligands, has thus been designed to compensate the large available surface and to enhance microsegregation auspicious to the formation of LC mesophases. The surface alteration of the native cluster $[Mn_{12}(OAc)_{16}]$ is achieved by the complete exchange of the 16 acetates with suitable benzoate-based ligands, a method extensively exploited to modify at wish the outer shell of the cluster, preserving at the same time the original single molecular magnetic behavior,[7,12] and recently shown efficient in promoting mesomorphism.[32,38] Since these earlier reports, other related strategies based on either covalent binding or ionic self-assembly (ISA) have successfully been employed to induce LC properties in a priori other nonmesogenic, three-dimensional hybrid molecular structures such as decaadduct-fullerene[39] derivatives, nanometer-sized organometallic[40] and highly charged polyoxometallate[41] clusters, and, to some extent, nanoparticular systems,[42] to name a few.

Mesomorphic, dodecanuclear manganese oxocomplexes with the general formula $[Mn_{12}O_{12}(L_{x,y,z\text{-CB}})_{16}(H_2O)_4]$ were therefore directly obtained by the complete replacement of the 16 LC-inert acetate groups of the precursory $[Mn_{12}(OAc)_{16}]$ compound with several proto-mesogenic cyanobiphenyl-containing benzoates, differing in the substitution pattern at the anchoring benzene ring, by solvent-mediated ligand-exchange reaction ($HL_{x,y,z\text{-CB}}$, Scheme 1). To ensure phase formation, the anchoring part was further decoupled from the mesogenic end-groups by undecylene spacers. $[Mn_{12}(OAc)_{16}]$ was prepared in situ from the easily accessible $MnOAc_2$ and $KMnO_4$ precursors, according to the standard procedure,[10] and the $HL_{x,y,z\text{-CB}}$ acid derivatives were prepared following literature protocols.[32,43]

Synthesis and Characterization of Ligands $HL_{x,y,z\text{-CB}}$ and Corresponding Dodecanuclear Clusters $[Mn_{12}O_{12}(L_{x,y,z\text{-CB}})_{16}(H_2O)_4]$. Acids $HL_{3,5\text{-CB}}$, $HL_{3,4\text{-CB}}$, and $HL_{4\text{-CB}}$ were prepared in two steps starting by the Williamson etherification of the precursory 3,5-dihydroxybenzoate, 3,4-dihydroxybenzoate, and 4-hydroxy-benzaldehyde, respectively, with 4′-(11-bromo-undecyloxy)-biphenyl-4-carbonitrile in acetone following published procedures ($HL_{3,4,5\text{-CB}}$ was reported pre-

Scheme 2[a]

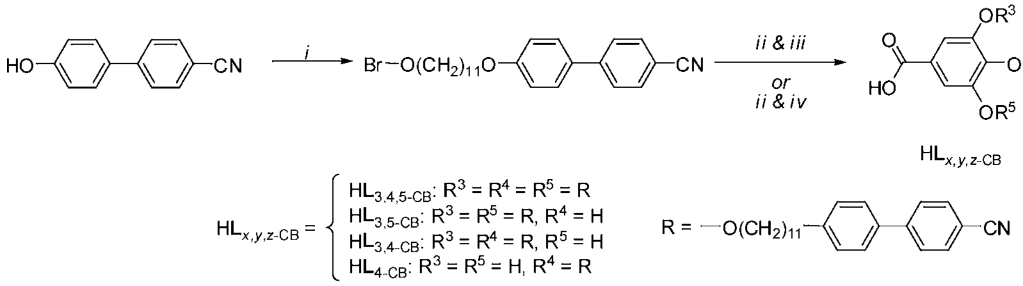

[a]Synthetic conditions: (i) Br-$(CH_2)_{11}$-OH, PPh_3, DIAD, THF, 0 °C → room temperature; (ii) 3,4,5-trihydroxybenzoate/3,5-dihydroxybenzoate/3,4-dihydroxybenzoate/4-hydroxy-benzaldehyde, K_2CO_3, KI_{cat}, acetone; (iii) KOH, EtOH/THF, H_2O, HCl 37%; (iv) H_2NSO_3H, $NaClO_2$, H_2O/THF.

viously).[32,43] The methyl esters Me$\mathbf{L}_{3,5\text{-CB}}$ and Me$\mathbf{L}_{3,4\text{-CB}}$ were hydrolyzed into their corresponding carboxylic acids, whereas the intermediate aldehyde derivative (Ald$\mathbf{L}_{4\text{-CB}}$) was directly converted into its acidic counterpart by treatment with the oxidizing $H_2NSO_3H/NaClO_2$ mixture (Scheme 2).

MS and elemental analyses probed the purity of all of the cyanobiphenyl-containing organic derivatives (Supporting Information). ^{1}H NMR confirmed the expected dynamically averaged C_{2v} molecular symmetry of H$\mathbf{L}_{3,5\text{-CB}}$ and H$\mathbf{L}_{4\text{-CB}}$, and the C_S symmetry of H$\mathbf{L}_{3,4\text{-CB}}$, on the ^{1}H NMR time scale. The liquid-crystalline properties of cyanobiphenyl-containing ligands and related precursors were studied by polarized-light optical microscopy (POM) and differential scanning calorimetry (DSC). This analysis revealed the formation of a metastable nematic (monotropic N) mesophase for all of the ligands, except for H$\mathbf{L}_{4\text{-CB}}$ whose mesophase is enantiotropic (Supporting Information), in agreement with published results on related compounds.[43] The clearing temperatures of the ligands decrease with increasing substitution, from 193 °C (H$\mathbf{L}_{4\text{-CB}}$) to 145−150 °C (H$\mathbf{L}_{3,5\text{-CB}}$ and H$\mathbf{L}_{3,4\text{-CB}}$) and 141 °C for H$\mathbf{L}_{3,4,5\text{-CB}}$ (Supporting Information). All of the acids are stable above their clearing temperatures.

The covalent functionalization of the dodecanuclear clusters' outer shell was achieved by ligand-exchange reaction between the parent $[Mn_{12}(OAc)_{16}]$ cluster with a large excess of the pro-mesogenic acids H$\mathbf{L}_{x,y,z\text{-CB}}$ mediated in a CH_2Cl_2/toluene solvent mixture (Scheme 1). After several successive azeotropic distillations of the produced CH_3CO_2H in toluene (to displace favorably the equilibrium), the crude hybridized clusters $[Mn_{12}O_{12}(\mathbf{L}_{x,y,z\text{-CB}})_{16}(H_2O)_4]$ were purified by gel exclusion chromatography (GPC) and obtained as room-temperature waxy solids after vacuum drying. The structural characterization of the clusters was performed in both solid state and solution, relying mostly on elemental analysis, found to be in good agreement with the expected stoichiometries, and by IR spectroscopy, whose full substitution of the 16 coordination sites, as well as complete removal of ligands in excess, was clearly established (Supporting Information). Once covalently grafted onto the clusters, the characteristic stretching vibration band of the carbonyl groups of the free benzoates disappeared; this absence also indicates that no free ligand or acetate was present.

Because the presence of the paramagnetic manganese ions, NMR spectroscopy is a priori not well suited (i.e., non quantitative). Indeed, the dipolar coupling between protons and d-electrons induces fast relaxation times. Consequently, serious broadening of the signals and possible unexpected shifts likely preclude proper peaks attribution. Moreover, the nonequivalency of the 16 binding sites (i.e., axial and equatorial positions, vide supra) and the possible occurrence of several positional (e.g., water molecules coordination mode) and conformational isomers (e.g., as in the case of low-symmetrical ligands such as H$\mathbf{L}_{3,4\text{-CB}}$) pose serious limitations. However, because dipolar coupling is distance-dependent, the peripheral protons of the cyanobiphenyl end-moieties will be less affected than those of the anchoring benzoate, and closer to the paramagnetic cluster metallic core, this technique may be used as a probe of their binding. Peripheral aromatic systems of the cyanobiphenyl units are thus particularly well adapted to this analysis: their signals are located in a chemical-shift range free of other peaks, and moreover are weakly broadened and shifted compared to those of the benzoate anchor. The NMR spectra of H$\mathbf{L}_{4\text{-CB}}$ and its corresponding $[Mn_{12}O_{12}(\mathbf{L}_{4\text{-CB}})_{16}(H_2O)_4]$ complex, both selected as excellent representatives of this effect, were measured in $CDCl_3$ and prove the binding of the benzoates onto the cluster (Figure 2, spectra of the other compounds are in the Supporting Information). The signals of the two sets of protons H_{1-2} have totally disappeared, a consequence of their grafting, and thus proximity to the paramagnetic cluster. In contrast, the presence of sets of protons H_{3-6} signals at same chemical shifts, although broadened, confirmed the grafting of the new ligands onto the cluster and in addition the complete absence of free ligand. Similar results were obtained for the other cyanobiphenyl-containing systems (Supporting Information).

Mesomorphic Properties of the Dodecamanganese Clusters. Liquid-crystalline mesophases were induced in the four hybrids upon heating as revealed by POM, DSC, and small-angle X-ray scattering (SAXS) techniques. The thermal behavior, structural data, and mesophase characteristics are collected in Table 1. As verified by thermogravimetry (TGA, Supporting Information), all clusters possess an enhanced thermal stability with respect to the precursory acetate parent (which decomposes at ca. 35 °C, in air), but decomposition still occurs at high temperatures in the mesophase before reaching the isotropic liquid phase: the onset of a continuous weight-loss is variable and depends on the sample structure, and occurs at about 150 °C for $[Mn_{12}O_{12}(\mathbf{L}_{4\text{-CB}})_{16}(H_2O)_4]$ and at ca. 200 °C for the three other cluster compounds; a weight loss greater than 2% is nevertheless not observed below 250 °C. Thus, providing that the compounds are not maintained for long periods of time above 150 °C, temperature-dependent analyses can be performed. POM observations carried out during the first heating are not very conclusive, and the presence of

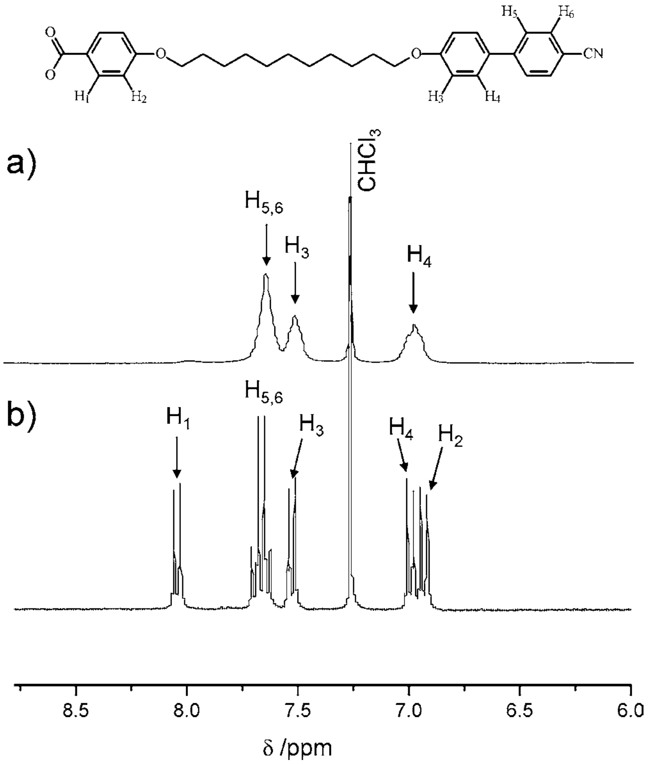

Figure 2. ^{1}H NMR spectra with numbering scheme for $[Mn_{12}O_{12}(\mathbf{L}_{4\text{-CB}})_{16}(H_2O)_4]$ (top) and $H\mathbf{L}_{4\text{-CB}}$ (bottom) in $CDCl_3$ at 298 K.

nonhomogeneous areas complicated a proper analysis. As for $[Mn_{12}O_{12}(\mathbf{L}_{3,4,5\text{-CB}})_{16}(H_2O)_4]$ previously described,[32] virgin samples needed to be heated first, then annealed for 1/2 min at high temperatures (e.g., 80−120 °C), and then cooled. After this thermal treatment, POM observations of the three new clusters revealed persistent, highly birefringent, and homogeneous optical textures (Supporting Information) in accordance with liquid-crystalline mesophase formation at or near room temperature, the fluidity of which increases as the temperature is raised. Phase assignment by this method appeared however adventurous, as no specific natural texture could be obtained because all of the clusters degrade before reaching the isotropic liquid (TGA). DSC thermograms were qualitatively similar for all compounds and in agreement with POM observations: during the first heating (and below 150 °C), weak and broad exo- and endothermic signals were obtained, confirming complicated thermal history and phase coexistence behaviors. Such complicated thermal behavior is commonly observed for intricate supermolecular systems such as oligomers, polypedes, and dendrimers.[30,44] On subsequent heating−cooling cycles, however (providing the decomposition temperatures were not attained), DSC traces appeared mostly silent, and a glass transition, corresponding to the freezing of the mesophase, was systematically observed at low temperatures (Supporting Information).

Temperature-dependent, small-angle X-ray diffraction experiments (performed between 40 and 150−200 °C) permitted one unequivocally to confirm the formation and nature of the LC mesophases for these systems, and to follow the evolution of the phase parameters with temperature (Supporting Information). Experiments carried out during the first heating revealed phases coexistence in the low-temperature ranges consequently to low-kinetics transformations (i.e., coexistence of a glassy LC phase and partially crystalline solid), consistent with DSC and POM analyses, as evidenced by the presence of several sharp, small- and large-angle reflections and broad signals, particularly true for $[Mn_{12}O_{12}(\mathbf{L}_{3,4,5\text{-CB}})_{16}(H_2O)_4]$ and $[Mn_{12}O_{12}(\mathbf{L}_{3,5\text{-CB}})_{16}(H_2O)_4]$. Upon continuing heating (between ca. 80−120 °C), the abrupt complete disappearance of one set of sharp reflections, those likely reminiscent of a residual crystalline ordering, is observed, giving rise to diffuse features, whereas another set of two sharp, small-angle reflections still remains over the whole temperature range. Once the samples were annealed for a few minutes in this 80−120 °C temperature range to allow the complete melting of the residual solid, clear diffractograms were obtained reversibly on subsequent temperature cycles. To allow comparison, the same thermal treatment was applied to the four samples, and in the following, only data obtained from the second and third temperatures cycles will be considered (no sign of degradation being detected).

As expected, all dodecanuclear compounds self-organize into lamellar smectic phases because the pending mesogens are typical calamitic smectogens,[29] and despite the different ligands substitution patterns, the smectic phases possess a similar structure. As general features, all temperature-dependent diffractograms are quite similar in all cases, showing sharp reflections in the small-angle region, indicative of some long-

Table 1. Thermal Transitions (Onset Temperatures) and Mesophase Characteristics for the Four LC SMM Compounds

L in cluster $[Mn_{12}O_{12}(\mathbf{L})_{16}(H_2O)_4]$	transition temp (°C)[a]	mesophase parameters[b]
$\mathbf{L}_{3,4,5\text{-CB}}$	G_{Sm} 40.5 Sm 200 dec.	T = 80−160 °C d = 41.9 ± 0.1 Å $h_{cluster}$ = 23.6 ± 1.0 Å V_{mol} = 34 000 ± 500 Å^3 ($\delta \approx 1$ g cm^{-3}) A_{mol} = 810 Å^2, a_{mes} = 33.8 Å^2
$\mathbf{L}_{3,5\text{-CB}}$	G_{Sm} 16.3 Sm 200 dec.	T = 40−140 °C d = 43.5 ± 0.1 Å $h_{cluster}$ = 20.2 ± 2.0 Å V_{mol} = 25 100 ± 500 Å^3 ($\delta \approx$ 0.96 g cm^{-3}) A_{mol} = 580 ± 20 Å^2, a_{mes} = 36.1 Å^2
$\mathbf{L}_{3,4\text{-CB}}$	G_{Sm} 17.0 Sm 200 dec.	T = 40−200 °C d = 45.3 ± 0.1 Å $h_{cluster}$ = 20.9 ± 2.0 Å V_{mol} = 24 000 ± 500 Å^3 ($\delta \approx 1$ g cm^{-3}) A_{mol} = 530 ± 20 Å^2, a_{mes} = 33.1 Å^2
$\mathbf{L}_{4\text{-CB}}$	G_{Sm} 17.2 Sm 150 dec.	T = 40−140 °C d = 47.0 ± 0.1 Å $h_{cluster}$ = 19.0 ± 3.0 Å V_{mol} = 14 000 ± 300 Å^3 ($\delta \approx$ 1.03 g cm^{-3}) $A_{mol} \approx$ 300 Å^2, a_{mes} = 37.2 Å^2

[a] Transition temperatures given from the second DSC cycle. Abbreviations: G_{Sm}, glassy smectic phase; Sm, smectic phase; dec, decomposition. [b] d, smectic periodicity; $h_{cluster}$, intercluster distance in the smectic sublayer, measured by XRD; V_{mol}, molecular volume; δ, density; A_{mol}, molecular cross-section area: $A_{mol} = V_{mol}/d$; a_{mes}, transverse cross-section area per mesogenic unit: $a_{mes} = 2A_{mol}/n_{mes}$ (n_{mes}: number of cyanobiphenyl subunits per cluster). All XRD were performed during the second and third heating cycles.

range order supramolecular lattices, and two sets of intense and diffuse signals with average maxima located at around 4.5−4.6 Å in wide-angle range, reflecting the liquid-like state of the molten alkyl chains and the average packing of the disordered diverging mesogenic subunits ($h_{\mathrm{ch+mes}}$, Figure 3), and between ca. 19−24 Å, provisionally associated with a ribbon periodicity and with the average correlation distance between first neighboring scattering polymetallic centers within the layers (h_{cluster}, Figure 3 and Table 1); the mesophases can thus be viewed as fluid and rather disordered (no in-plane ordering of the peripheral mesogenic units). The layer periodicities are directly given by the position of the two sharp and equidistant small-angle reflections in the spacing ratio 1:2, indexed with the 001 and 002 Miller indices (00*l*) (Table 2, Figure 3, Supporting Information). The periodicities are of the same magnitude, ranging between 42 and 47 Å (Table 1), and decrease linearly as the number of pending cyanobiphenyl groups is changed from 16 ($[\mathrm{Mn_{12}O_{12}}(\mathbf{L}_{4\text{-CB}})_{16}(\mathrm{H_2O})_4]$) to 48 ($[\mathrm{Mn_{12}O_{12}}(\mathbf{L}_{3,4,5\text{-CB}})_{16}(\mathrm{H_2O})_4]$) via 32 ($[\mathrm{Mn_{12}O_{12}}(\mathbf{L}_{3,x\text{-CB}})_{16}(\mathrm{H_2O})_4]$, x = 4, 5) due to the overall molecular lateral expansion (Figures 3 and 4). This trend is a priori connected to specific packing constraints and dipolar interactions between the cyanobiphenyl units (vide infra). For each compound, the lamellar periodicity is also quasi-invariant with temperature (less than a few %), suggesting little effect of the temperature on the supramolecular arrangements (Supporting Information).

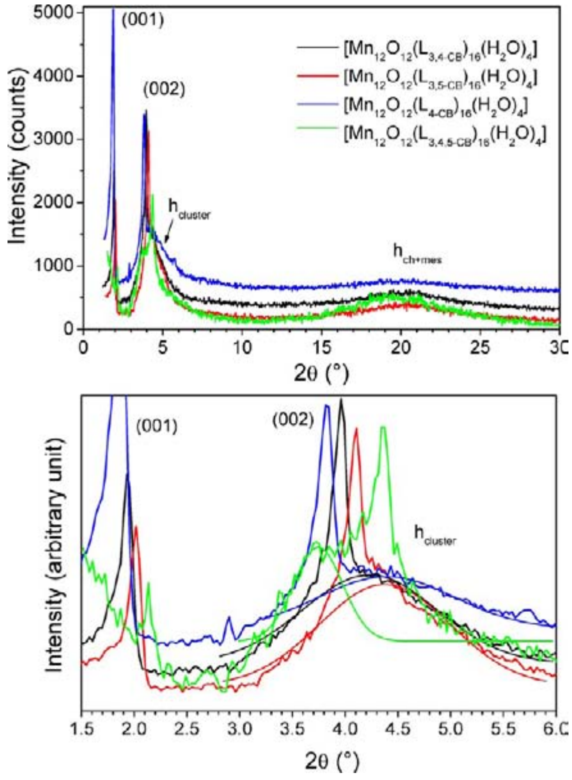

Figure 3. Representative X-ray patterns of the three new clusters recorded at 80 °C and of $[\mathrm{Mn_{12}O_{12}}(\mathbf{L}_{3,4,5\text{-CB}})_{16}(\mathrm{H_2O})_4]$ at 120 °C (top) and enlargement of the 1.5−6° 2θ-zone (bottom). Thin lines are fits of the broad diffusion line (h_{cluster}) with a Gaussian function (see text).

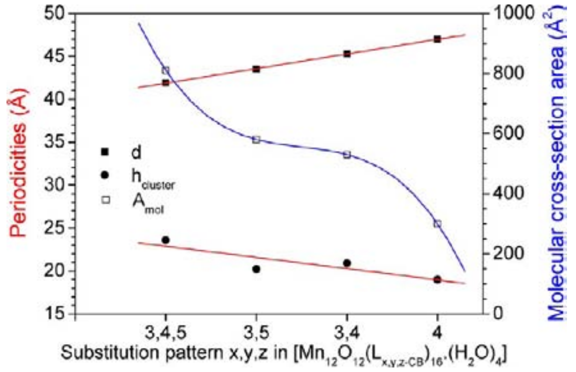

Figure 4. Plots of the relevant mesophase parameters as a function of the substitution pattern of the Mn12 complexes.

The abnormal intensity profile of the two reflections, with a relatively weak (001) reflection with respect to (002), is a strong indication of segregation occurring at the molecular level between the cluster, the mesogens, and the aliphatic spacers, respectively. Such an intensity distribution indeed arises from the modulation of the electronic density within the lamellar periodicity produced by the regular alternation of high- and low-electronic density sublayers, and particularly here is testimony (due to the enhanced 002 reflection) of an increase of the electronic density in the central slab of the layer, containing the strongly scattering polymetallic central cores. Note that the variation of the relative intensities ratio observed for the four complexes differs slightly and obviously depends on the respective thickness ratios of their different sublayers (due to the ligand substitution pattern), and on the sharpness of the various interfaces. No obvious other change could be observed

Table 2. Comparison of the Mean Distance between First Neighboring Clusters for Ideal Hexagonal and Square Symmetrical Arrangements, XRD Values, and Molecular Dynamic Values[a]

		hexagonal symmetry			square symmetry			h		
L in cluster $[\mathrm{Mn_{12}O_{12}}(\mathbf{L})_{16}(\mathrm{H_2O})_4]$	A_{mol}	h_{min}	$\langle h_{\mathrm{hex}}\rangle$	h_{max}	h_{min}	$\langle h_{\mathrm{sq}}\rangle$	h_{max}	h_{cluster}	h_{md}(sq)	h_{md}(hex)
$\mathbf{L}_{3,4,5\text{-CB}}$	810	26.48	27.78	30.6	20.12	22.58	28.46	23.6 ± 1.0	28.4	30.5
$\mathbf{L}_{3,5\text{-CB}}$	580	22.4	23.51	25.9	17.03	19.11	24.08	20.2 ± 2.0	23.0	−
$\mathbf{L}_{3,4\text{-CB}}$	530	21.4	22.47	24.74	16.28	18.27	23.02	20.9 ± 2.0	−	−
$\mathbf{L}_{4\text{-CB}}$	300	16.11	16.91	18.6	12.25	13.75	17.32	19.0 ± 3.0	17.0	−

[a] Hexagonal symmetry: $A_{\mathrm{mol}} = h_{\mathrm{min}}\cdot h_{\mathrm{max}}$, $h_{\mathrm{max}}/h_{\mathrm{min}} = 2/\sqrt{3}$, and $\langle h_{\mathrm{hex}}\rangle = 3^{5/4}\log 3 \times \sqrt{A_{\mathrm{mol}}/[\pi\sqrt{2}]} = 0.9763\sqrt{A_{\mathrm{mol}}}$. Square symmetry: $A_{\mathrm{mol}} = (h_{\mathrm{max}})^2 = 2 \times (h_{\mathrm{min}})^2$, $h_{\mathrm{max}}/h_{\mathrm{min}} = \sqrt{2}$, $\langle h_{\mathrm{sq}}\rangle = 2\sqrt{2}\log(1 + \sqrt{2}) \times \sqrt{A_{\mathrm{mol}}/[\pi]} = 0.7935\sqrt{A_{\mathrm{mol}}}$; h_{cluster} was measured by SAXS; h_{md} was obtained from molecular dynamics considering a square lattice in all cases, and square and hexagonal lattices for $[\mathrm{Mn_{12}O_{12}}(\mathbf{L}_{3,4,5\text{-CB}})_{16}(\mathrm{H_2O})_4]$. $\langle h_{\mathrm{hex}}\rangle$ and $\langle h_{\mathrm{sq}}\rangle$ were determined according to the integral equation: $\langle h/h_{\mathrm{min}}\rangle = (\theta_2 - \theta_1)^{-1}\int d\theta/\cos\theta$, where θ_1 and θ_2 are the limits for the integration: $\theta_1 = 0$ and $\theta_2 = \pi/6$ and $\pi/4$ for the hexagonal and square symmetry, respectively; (−) modeling not performed.

in the X-ray patterns within the series of $[Mn_{12}O_{12}(\mathbf{L}_{x,y,z\text{-CB}})_{16}(H_2O)_4]$ clusters between 40 and 150/200 °C, except for a strong temperature- and structure-dependency of the relative intensity ratio of the two sharp reflections, I_{001}/I_{002}, which decreases on raising the temperature from approximately ca. 4:1 to 1:1 or 1:2 (or even lower, because the 001 reflection may be almost extinct); the phenomenon is completely reversible with temperature on subsequent heat−cool cycles (Figure 3).

Present for all samples, the small-angle broad diffusion (h_{cluster}, Figure 3), localized at the base of the sharp 002 reflection, and whose value is slightly larger than the average diameter of the naked cluster, corresponds indeed to a periodicity and to the short-range correlation distance between metallic centers within the lamellae. Confirming this assumption, the maximum of the diffusion, determined by fitting the experimental line shape with a Gaussian function, also varies linearly with the terminal mesogenic groups number (Figure 4), that is with the lateral molecular expansion. Furthermore, in the investigated mesomorphic temperature interval, this broad diffusion does not shift significantly, and the intensity of the signal remains more or less constant (Supporting Information).[45] The specific molecular structures and these observations strongly support that this diffusion actually belongs to a periodicity produced by the disruption of the aliphatic sublayer by the hard-core cluster; in other words, this signal arises from the modulation of the electronic density in the sublayer consequent to the embedment of the highly scattering clusters within the low-electron density aliphatic continuum. Moreover, the relative broadness of the signal indicates some limited and short-range in-plane correlations between the cluster cores within the layer, such as, first neighbor's type correlation, obviously not correlated with adjacent layers (no 3D correlations).

Therefore, despite the structural variations within the members of the series, all of the diffractograms recorded in the mesophases temperature ranges look similar (Figure 3), suggesting that the same mesophase structure is kept in the whole series. As found for structurally related hybridized molecular systems of this type,[32,36−38,40,41] the mesophase can thus be satisfactorily described by a smectic morphology, consisting of a bilayer structure made of outer mesogens sublayers with a short-range 2D in-plane arrangement of the clusters embedded in the median aliphatic sublayer (vide infra).

As far as the local packing is concerned, subtle differences depending on the compounds can be revealed, which are evidently associated with the various ligands substitution pattern topologies and consequently with the number/position of appending mesogens connected to the clusters. These modifications within the series can be appreciated by following the evolution of the molecular areas, A_{mol}, deduced from the ratio between the molecular volumes (V_{mol}), calculated with a density of 1.00 ± 0.05 g cm^{-3} (Table 1), and the mean layer thickness (d). As expected, the molecular area is found to increase concomitantly with the number of end-mesogens, evidencing the bulkiness of the periphery in comparison to the cluster hard-cores (Figure 4). These values also prompt that the fundamental lamellar periodicities therefore correspond to one monomolecular bilayer, induced by the lateral two-dimensional registry of the molecules in pseudocylindrical conformation, that is, with one-half of the mesogenic pending arms distributed on either side of the median molecular plane, all pointing on average along the same direction (Figure 5). The mesogenic transverse cross-section area, a_{mes} ($a_{\text{mes}} = 2A_{\text{mol}}/n_{\text{mes}}$ with n_{mes} = total number of cyanobiphenyl units per cluster, Table 1), reveals a strong substitution-dependent compactness with values ranging around 33 Å^2 for $[Mn_{12}O_{12}(\mathbf{L}_{3,4,5\text{-CB}})_{16}(H_2O)_4]$ and $[Mn_{12}O_{12}(\mathbf{L}_{3,4\text{-CB}})_{16}(H_2O)_4]$ to about 37 Å^2 for $[Mn_{12}O_{12}(\mathbf{L}_{3,5\text{-CB}})_{16}(H_2O)_4]$ and $[Mn_{12}O_{12}(\mathbf{L}_{4\text{-CB}})_{16}(H_2O)_4]$ (Table 2). First, all of these values are significantly larger than the theoretical cross section of an aliphatic chain (22.5 Å^2), expected in the ideal case of long-range lateral packing of mesogens, parallel to the layer normal as in a classical SmA phase. Such divergences usually originate from the combination of partial mesogens' interpenetration between adjacent layers and/or from a substantial tilt of the rigid cores with respect to the layer's normal, leading to undulated interfaces. Second, and specifically here, divergences also result from the nonequivalence of the connecting sites around the rigid and nondeformable cluster core, axial and equatorial positions, which also contribute substantially to the variation of the transverse area.

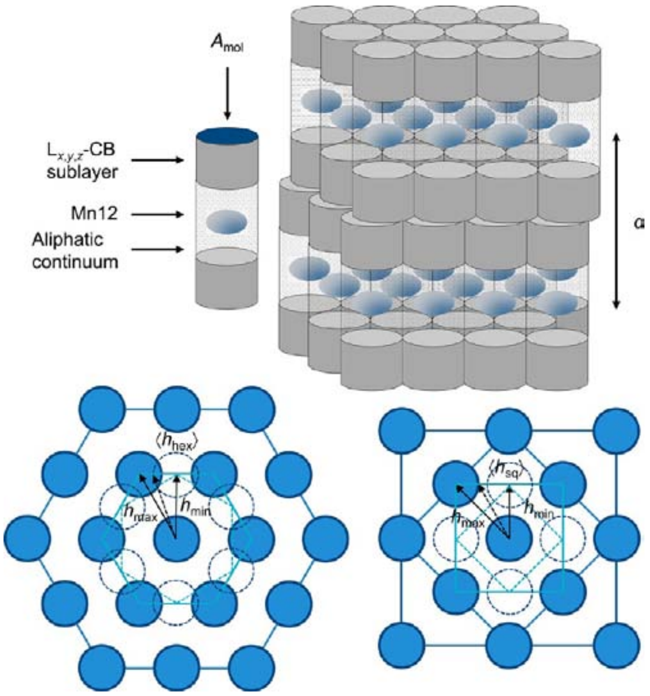

Figure 5. Top: Schematic representation of the cylindrical shape ($d \times A_{\text{mol}}$) of the hybrids and perspective view of the self-organization of the Mn12 complexes into smectic layers. Bottom: Representations of the two in-plane lattices (hexagonal and square symmetry, respectively) for the 2D arrangements of the clusters within the median sublayer and description of the relevant geometrical parameters (the blue circles represent the time-averaged circular projection of the cluster onto the lattice plane, the dotted circles for the dual lattices, and the white parts the aliphatic continuum; the solid and dotted light-blue lines represent the large and small (dual) lattices of these arrangements, and the darker solid lines represent the first neighbors' lattice); h_{max} and h_{min} (black arrows) represent the maximum and minimum distances between two nodes within the lattice plane (hexagonal and/or square symmetry, i.e., the parameters of the large and small (dual) lattices respectively); $\langle h_{\text{hex}}\rangle$ and $\langle h_{\text{sq}}\rangle$ (black dotted arrows) represent the average distances between lattice nodes (see Table 2).

Clearly, the bulkier is the periphery, the more densely the peripheral substituents are laterally close-packed in the sublayers. Indeed, the polysubstituted systems, $[Mn_{12}O_{12}$-

$(\mathbf{L}_{3,4,5\text{-CB}})_{16}(H_2O)_4]$ and $[Mn_{12}O_{12}(\mathbf{L}_{3,4\text{-CB}})_{16}(H_2O)_4]$, show a stronger tendency than do the less crowded ones, $[Mn_{12}O_{12}(\mathbf{L}_{4\text{-CB}})_{16}(H_2O)_4]$ and $[Mn_{12}O_{12}(\mathbf{L}_{3,5\text{-CB}})_{16}(H_2O)_4]$ (because of the nonoccupied meta or para positions, respectively) to depart from the sublayers formed by the mesogens connected at the axial ones, essentially by pulling those connected at the equatorial positions, reducing the average molecular area per mesogen relatively (Table 1). Interestingly, the two constitutional isomers, $[Mn_{12}O_{12}(\mathbf{L}_{3,5\text{-CB}})_{16}(H_2O)_4]$ and $[Mn_{12}O_{12}(\mathbf{L}_{3,4\text{-CB}})_{16}(H_2O)_4]$, behave quite differently, and this behavior seems to concord with the numerous possible conformations adopted for the latter compound (consequent to its nonsymmetrical substitution pattern), which can, in a first approximation, be time-averaged with $[Mn_{12}O_{12}(\mathbf{L}_{3,4,5\text{-CB}})_{16}(H_2O)_4]$ compound. Thus, the evolution of the lamellar packing within the series is fairly well understood by considering altogether the number of pending mesogens (i.e., 48, 32, 16), the substitution pattern (i.e., 3,4,5-, 3,4-, 3,5-, and 4-), and the two connecting modes around the cluster (i.e., axial versus equatorial positions), all influencing at various levels areas and packing constraints.

As mentioned above, the segregated nature and cylindrical conformation of the hybrids (Figure 5) imply also that the bulky metallic hard-cores are somehow correlated in the median plane of the smectic layer. Unfortunately, discussion upon the exact lateral two-dimensional packing of central clusters within the correlated single layers could only be speculative, because only a diffuse signal (h_{cluster}, Figure 3) could be detected in the powder patterns; the correlation is only short-range, and extends to first neighbors only. Generally, and particularly here, the mean packing viewed by X-ray diffraction actually emerges from the local scale molecular packing, determined by interactions between neighboring molecules, molecular conformational changes, and motions, which is smoothed and averaged. Moreover, experiments on aligned samples did not yield oriented patterns of the mesophase, precluding the absolute assignment of the symmetry and orientation of this pseudolattice. In 2D self-assemblies, positional ordering is mostly hexagonal, but other periodic patterns such as square, pentagonal tiling, etc., or even binary tilling combinations, which increase further the possibilities, are possible.[30e,i] Whatever the symmetry considered for such a local arrangement, the geometry is determined by the molecular area, which defines the lattice area. In the present case, the molecules adopt a cylindrical shape, with a time-averaged circular cross-section, and therefore essentially the two likely possibilities of 2D patterning are square or hexagonal (Figure 5). The partial deciphering of the local packing and the estimation of $\langle h \rangle$, the mean average distance between the two closest adjacent circular surfaces, which in our case represents the average distance between two nearest clusters, were achieved by using a straightforward geometrical approach considering both hexagonal and square packing modes, corollary to the molecular cross-section areas, A_{mol}. Because the system is liquid-crystalline and thus fluid, the $\langle h \rangle$ distance ($\langle h_{\text{hex}} \rangle$ or $\langle h_{\text{sq}} \rangle$) fluctuates logically between two limit values, $h_{\min}$ and $h_{\max}$ ($h_{\max}$ is the largest distance and $h_{\min}$ is the shortest distance between two neighbors, for each symmetry considered, Figure 5). In fact, for each symmetry, $h_{\max}$ and $h_{\min}$ both correspond to the parameters of both the large and the small (dual) 2D lattices, respectively. The minimum and maximum ($h_{\min}$ and $h_{\max}$) and mean ($\langle h_{\text{sq}} \rangle$,$\langle h_{\text{hex}} \rangle$) distances between first neighbors are in general good agreement and comparable with the average distances between clusters measured by SAXS (h_{cluster}) for each sample. In addition, from these calculations, a slight trend toward the square lattice is revealed (Table 2, $h_{\text{cluster}} \approx \langle h_{\text{sq}} \rangle$) for all compounds, a likely consequence of the bulkiness of the periphery, except for the less crowded $[Mn_{12}O_{12}(\mathbf{L}_{4\text{-CB}})_{16}(H_2O)_4]$ (Table 2, $\langle h_{\text{hex}} \rangle \approx h_{\text{cluster}}$). When the number of mesogens is increased, the molecular area is dominated by the peripheral mesogens, leading to more compact arrangements and hindering the overall molecular rotation around the main molecular axis (compare A_{mol} and a_{mes} values in Table 1). In addition, due to the large number of susbstituents, the appending gallates irradiating from the core (equatorial positions) force the Mn12 clusters out of the median plane by pulling the mesogens toward the outer mesogenic sublayers (for $[Mn_{12}O_{12}(\mathbf{L}_{3,4,5\text{-CB}})_{16}(H_2O)_4]$ and $[Mn_{12}O_{12}(\mathbf{L}_{3,4\text{-CB}})_{16}(H_2O)_4]$). The combined effects of the hindered rotation, out of plane orientation, and equatorial crowding contribute to the local symmetry reduction and to the persistence of the overall 4-fold symmetry, and consequently lead here preferentially to a square-like arrangement. In the opposite situation, $[Mn_{12}O_{12}(\mathbf{L}_{4\text{-CB}})_{16}(H_2O)_4]$, the molecular area is less restricted by the periphery; the terminal mesogens and the less crowded equatorial benzoates have more freedom, and the cluster is not pulled out of the plane: this peculiar arrangement likely blurs the intrinsic S_4 symmetry of the cluster by smoothing the interface with the aliphatic continuum, and drives to both in-plane arrangements equally. For $[Mn_{12}O_{12}(\mathbf{L}_{3,5\text{-CB}})_{16}(H_2O)_4]$, the intermediate situation occurs (large a_{mes}, no tilted core, and large number of substituents).

Validation of this supramolecular arrangement was attempted by molecular modeling and molecular dynamic calculations. The simulation methods used here provide a snapshot of the conformations and arrangements of few-molecules models in a minimized energy status. The detailed procedure of the simulation[46] consisted of placing two molecules (two superimposed subsets of molecules), formerly optimized (e.g., with a more or less cylindrical shape), in an orthorhombic box and setting a constraint onto the molecular area A_{mol} deduced from X-ray data and volumetric calculations. The z parameter of the orthorhombic cell was set to 200 Å (much larger than twice the measured periodicity, Table 1) so as not to constrain the thickness artificially and to allow sufficiently large molecular motions for an efficient and reproducible optimization of the conformations and of the supramolecular arrangements. Each manganese atom of a given cluster was restricted to its position relative to the others within the metallic framework, according to the X-ray crystalline structure of the trimethoxy gallate homologous cluster,[32] whereas all other atoms were allowed to move freely, as were the two molecules in the constrained cell. Modeling results previously obtained for $[Mn_{12}O_{12}(\mathbf{L}_{3,4,5\text{-CB}})_{16}(H_2O)_4]$ supported this view of the self-assembly of highly segregated molecules into bilayer smectic phases, in good accordance with the diffraction parameters, and particularly they highlighted the good convergence of the lattice dimension toward the lamellar periodicity. Molecular dynamics further highlighted that all of the clusters cores were tilted out of the plane with respect to the median sublayer of the smectic phase with no tilt correlation within and between layers (random orientation), confirming the pulling effect of the peripheral mesogens. A square lattice was also preferred at that time with respect to the hexagonal lattice (only these two

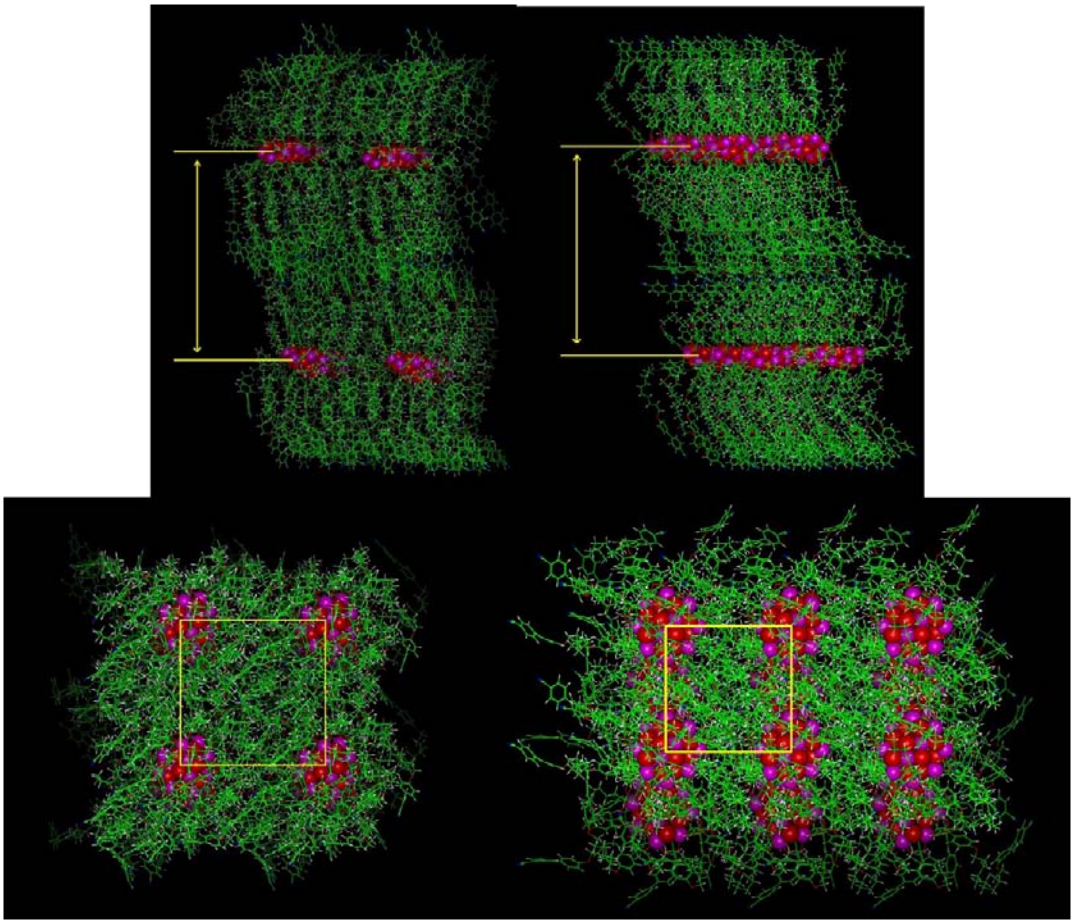

Figure 6. Side-views of the lamellar packing of the clusters (top) and top-views of the in-layer lateral arrangement of the clusters in square-like lattice (bottom): $[Mn_{12}O_{12}(\mathbf{L}_{3,5\text{-CB}})_{16}(H_2O)_4]$ (left) and $[Mn_{12}O_{12}(\mathbf{L}_{4\text{-CB}})_{16}(H_2O)_4]$ (right).

lattices were considered, vide supra), also in agreement with the overall intrinsic S_4 molecular symmetry of Mn12 complexes.[32]

New such simulations experiments were therefore performed on the symmetrical clusters $[Mn_{12}O_{12}(\mathbf{L}_{3,5\text{-CB}})_{16}(H_2O)_4]$ and $[Mn_{12}O_{12}(\mathbf{L}_{4\text{-CB}})_{16}(H_2O)_4]$ to confirm the bilayer nature of the structure, and eventually the nature of the lateral packing; the nonsymmetrical nature of the other cluster precluded such experiments. Some of the more relevant results of these calculations are displayed in Figure 6. After important oscillations in the beginning of the simulation, the amplitude of the layers fluctuations reaches a stable regime with thicknesses converging to the lamellar values measured by SAXS (Supporting Information), independent of the lattice considered. Molecular dynamics was able to discriminate between square and hexagonal lattices $[Mn_{12}O_{12}(\mathbf{L}_{3,5\text{-CB}})_{16}(H_2O)_4]$ (Figure 6) for which a good convergence was observed ($h_{\text{cluster}} \approx h_{\text{md}}(\text{sq}) = h_{\text{max}}(\text{sq})$ Table 2) by setting a square lattice, but unable to do so for $[Mn_{12}O_{12}(\mathbf{L}_{4\text{-CB}})_{16}(H_2O)_4]$ ($h_{\text{md}}(\text{sq}) = \langle h_{\text{hex}} \rangle$ and $h_{\text{cluster}} = h_{\text{max}}(\text{hex})$, Table 2), for which the registry in the third direction was necessary to reconcile the square arrangement with the molecular area. As assumed above, the reality probably is an average representation of both (expected by the broadness of the diffuse X-ray signals), presumably resulting from slight shifts in position (and orientation) between neighboring clusters, further blurred out by the dynamics of the liquid crystal phase (fluidity of the mesophase). Finally, for $[Mn_{12}O_{12}(\mathbf{L}_{3,5\text{-CB}})_{16}(H_2O)_4]$, molecular dynamics revealed that the clusters are not inclined out of the median plane, unlike for $[Mn_{12}O_{12}(\mathbf{L}_{3,4,5\text{-CB}})_{16}(H_2O)_4]$, but remain rather flat in the plane as for the less crowed system, $[Mn_{12}O_{12}(\mathbf{L}_{4\text{-CB}})_{16}(H_2O)_4]$, in agreement with the larger (and similar) values of a_{mes} (Table 1).

To conclude on the mesomorphic properties, all of the clusters self-organize at room temperature into smectic bilayers, with the clusters fully embedded in the central aliphatic sublayers, forming a weakly correlated 2D lattice. It was shown that the substitution pattern can be used as a means to control the packing density and stimulate the type of symmetry of the local 2D clusters arrangement (a_{mes}, tilting, equatorial crowding). Of particular interest, in the case of the densely packed systems, is the tendency of the equatorial mesogenic groups to reach the mesogenic sublayers, forcing the clusters out of plane and probably inducing important local structural distortions of the clusters.

Magnetic Properties of the Dodecanuclear Clusters $[Mn_{12}O_{12}(L_{x,y,z\text{-CB}})_{16}(H_2O)_4]$. The signature of SMM compounds is generally associated with the presence of a frequency-dependent out-of-phase ac susceptibility signal (χ'') that can be measured when the frequency of the ac field becomes close to the relaxation frequency of the molecule magnetic moment.[47] The ac magnetic susceptibility is also used to determine the spin of the ground state (assuming that only the ground state is populated at this temperature) as well as the height of the effective energy barrier (U_{eff}), which prevents the thermal relaxation of the magnetization. Indeed, the relaxation time of

Table 3. Magnetic Properties for $[Mn_{12}O_{12}(\mathbf{L}_{x,y,z\text{-CB}})_{16}(H_2O)_4]$

L in cluster $[Mn_{12}O_{12}(\mathbf{L})_{16}(H_2O)_4]$	relaxation modes[a]	T_B (K)[b]	μ_0H_C (T)[c]	S, g[d]	U_{eff} (K)[e]	τ_0 (s)[f]	JT isomeric ratio (SR/FR)
$\mathbf{L}_{3,4,5\text{-CB}}$	FR and SR	2.4	0.320	9, 1.91	55	1.4×10^{-8}	65/35
$\mathbf{L}_{3,5\text{-CB}}$	FR and SR	2.6	0.600	9, 1.99	60	8.4×10^{-9}	60/40
$\mathbf{L}_{4\text{-CB}}$	FR and SR	2.5	0.575	10, 1.88	59	6.2×10^{-9}	55/45
$\mathbf{L}_{3,4\text{-CB}}$	FR and SR	2.5	0.130	9, 1.87	59	4.4×10^{-9}	35/65

[a] SR: slow relaxing phase. FR: fast relaxing phase. The FR phases occur at too low temperature and/or are too weak to be fully characterized. [b] T_B: blocking temperature (arbitrary defined as corresponding to a relaxation time of 100 s for the SR species). [c] μ_0H_C: coercive field measured at T = 1.8 K. [d] S, g: spin and Lande factor of the ground state. [e] U_{eff}: potential energy barrier. [f] τ_0: pre-exponential factor.

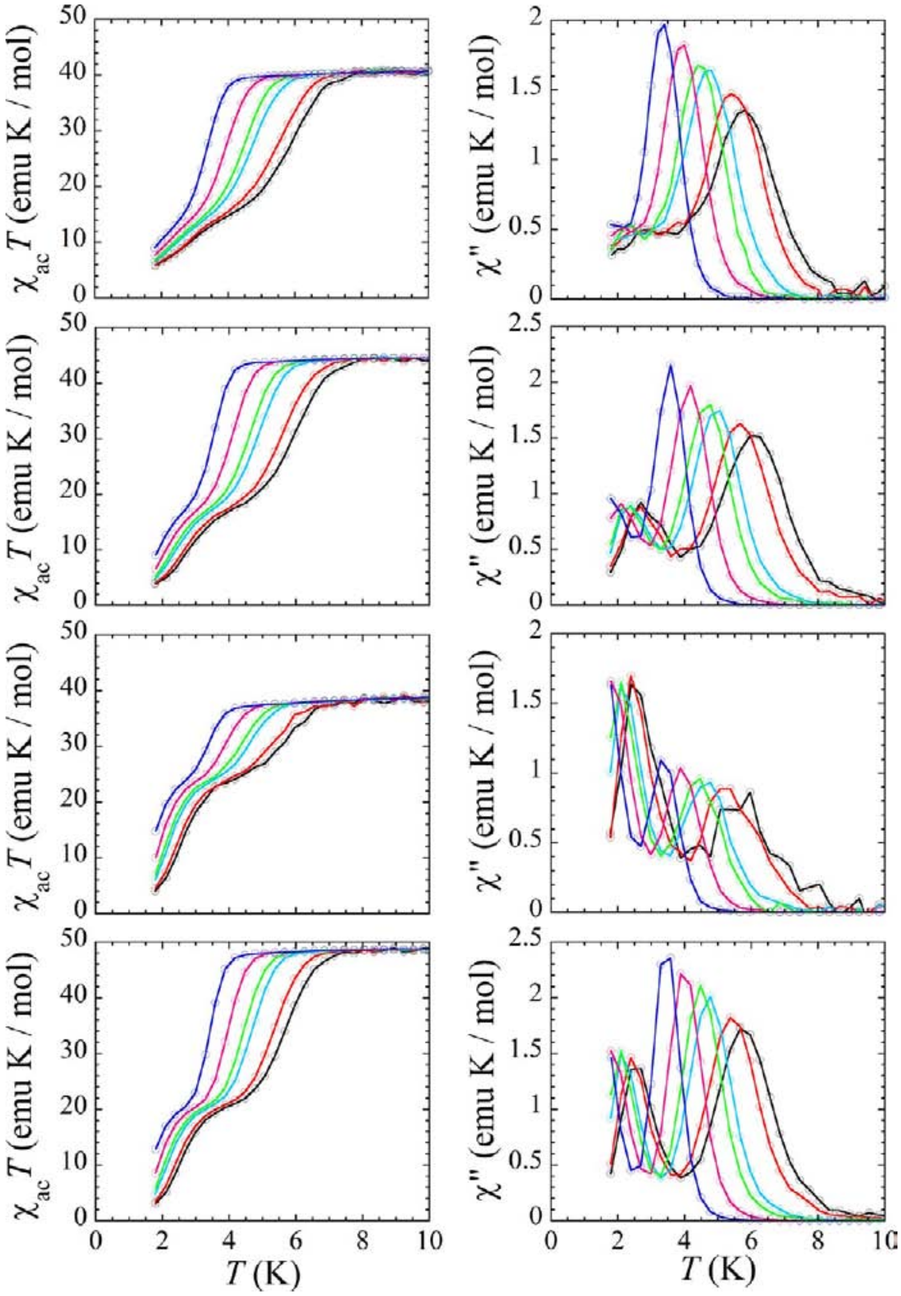

Figure 7. Temperature dependence of $\chi_{ac}T$ (left column) and χ'' (right column) for, from top to bottom, $[Mn_{12}O_{12}(\mathbf{L}_{3,4,5\text{-CB}})_{16}(H_2O)_4]$, $[Mn_{12}O_{12}(\mathbf{L}_{3,5\text{-CB}})_{16}(H_2O)_4]$, $[Mn_{12}O_{12}(\mathbf{L}_{3,4\text{-CB}})_{16}(H_2O)_4]$, and $[Mn_{12}O_{12}(\mathbf{L}_{4\text{-CB}})_{16}(H_2O)_4]$. $\chi_{ac} = (\chi'^2 + \chi''^2)^{0.5}$, with χ' and χ'' being, respectively, the real and imaginary components of the molar magnetic susceptibility ($\chi = \chi' + i\chi''$) at zero dc field with a field of 3.5 Oe oscillating at 1000 (black), 500 (red), 100 (cyan), 50 (green), 10 (magenta), and 1 Hz (dark blue).

SMM magnetization usually follows a thermally activated process that can be described by the Arrhenius law ($\tau = \tau_0 \exp(-U_{eff}/k_BT)$, where τ is the relaxation rate, k_B is the Boltzmann constant, and τ_0 is a pre-exponential factor), making thus possible the determination of the blocking temperature (T_B, arbitrarily defined as corresponding to a relaxation time of 100 s). For $[Mn_{12}(OAc)_{16}]$, the parameters used to fit the Arrhenius type dependence of the relaxation time of the magnetization, τ, are: $\tau_0 = 2.1 \times 10^{-7}$ s and $U_{eff}/k_B = 61$ K.[15] This means that the relaxation time of the magnetization of $[Mn_{12}(OAc)_{16}]$ is of the order of months at 2 K. The fact that the low-temperature slow relaxation of the magnetization of SMM occurs at the molecular level and does not result from collective interactions has been experimentally established, in particular with low-temperature calorimetry (no specific heat anomaly) and magnetometry on diluted samples. As none of the clusters involved in this study could be obtained as large single crystals, essentially because of the constitutive flexible and mesomorphous organic coating, the study of the magnetic properties was performed on powder samples instead, still admitting the hypothesis of the above relaxation pathway. The same thermal treatment as described above (SAXS) was applied here before carrying magnetic measurements to bring the samples in the same homogeneous state, and thus to eventually allow precise structural comparisons. Note that prior magnetic measurements performed without thermal treatment gave very similar results, and the values found in this set of compounds are in good agreement with what is usually found for Mn12 clusters, suggesting that (i) the integrity of the clusters is preserved during thermal annealing, and (ii) the coexisting smectic mesophase and partially crystallized solid (vide supra) likely possess a similar type of supramolecular lamellar (pre)organization. All of these parameters gained from χ'' and $\chi_{ac}T$ ($\chi_{ac} = (\chi'^2 + \chi''^2)^{1/2}$) versus T and magnetization hysteresis cycles measurements are summarized in Table 3 (and Supporting Information). In Figure 7, plots of $\chi_{ac}T$ product and χ'' versus T at various oscillating frequencies (from 1 kHz to 1 Hz) are displayed. The frequency-dependent decrease in the $\chi_{ac}T$ versus T plot on lowering the temperature, observed in all four Mn12 derivatives, indicates that the relaxation of the magnetization rate becomes close to the ac field frequency. Accordingly, a χ'' signal appears at the corresponding temperature, indicating SMM behavior for all of the Mn12-based materials.

For the three novel compounds, the $\chi_{ac}T$ values above 8 K are equal and constant at all frequencies. Assuming that only the ground state is populated at this temperature, the value of the $\chi_{ac}T$ product can be used to determine the spin of the ground state of the clusters. The values of the $\chi_{ac}T$ products measured at the plateau were 44.5, 39.5, and 48.8 emu K mol^{-1}, leading to $S = 9$ and $g = 1.99$, $S = 9$ and $g = 1.87$, and $S = 10$ and $g = 1.88$ for $[Mn_{12}O_{12}(\mathbf{L}_{3,5\text{-CB}})_{16}(H_2O)_4]$, $[Mn_{12}O_{12}(\mathbf{L}_{3,4\text{-CB}})_{16}(H_2O)_4]$, and $[Mn_{12}O_{12}(\mathbf{L}_{4\text{-CB}})_{16}(H_2O)_4]$, respectively, in fair accordance with those determined for other Mn12-based complexes: even though most of them possess a $S = 10$ spin ground state, systems with $S = 9$ are not rare and have been measured in many cases (vide supra).[48] Recall that for $[Mn_{12}O_{12}(\mathbf{L}_{3,4,5\text{-CB}})_{16}(H_2O)_4]$, the value of $\chi_{ac}T$ at the plateau was around 41 emu K mol^{-1}, corresponding to a ground state of $S = 9$ and $g = 1.91$.[32] The onset of a second plateau is observed at lower temperatures ($\chi_{ac}T \leq 20$ emu K mol^{-1}, Figure 7).

As evidenced by the presence of two plateaus in the $\chi_{ac}T$ versus T products and two peaks in the χ'' versus T plots, two frequency-dependent out-of-phase ac susceptibility signals were also observed for the four compounds $[Mn_{12}O_{12}(\mathbf{L}_{x,y,z\text{-CB}})_{16}(H_2O)_4]$, suggesting two different relaxation processes, the first one in the region 4−8 K, corresponding to a slow relaxation mode (SR), and the other one in the region 1−3 K, corresponding to a fast relaxation mode (FR) (Figure 7). The occurrence of two peaks in the out-of-phase susceptibility is not an unusual feature for Mn12 derivatives.[49] A well-accepted explanation for the presence of two relaxation modes is due to subtle structural differences in the molecular structures, not damaging the clusters. One structural difference may arise from the position of the four water molecules coordinated to type II Mn^{III} ions,[11,48,50,51] but the most significant difference at the origin of these two relaxation modes is attributed to JT isomerism, due to the splitting of the degenerate d orbitals of the Mn^{III} ions (d^4) in octahedral ligand field (O_h), which elongation leads to a tetragonal geometry (D_{4h}).[19] At this stage, because no crystallographic structure is available, we propose the hypothesis that the presence of these two peaks is principally caused by the coexistence of JT isomers within each sample. The ratio of each isomer can be approximately determined by the difference of the two plateaus present in $\chi_{ac}T$ versus T plots. The SR/FR ratios measured are ca. 65/35, 60/40, 55/45, and 35/65 for Mn12 systems with ligands substitution in the decreasing sequence $\mathbf{L}_{3,4,5\text{-CB}}$, $\mathbf{L}_{3,5\text{-CB}}$, $\mathbf{L}_{4\text{-CB}}$, and $\mathbf{L}_{3,4\text{-CB}}$, respectively.

The dynamic magnetic behavior of the complexes $[Mn_{12}O_{12}(\mathbf{L}_{x,y,z\text{-CB}})_{16}(H_2O)_4]$ seems to be somehow influenced by the overall molecular structure, that is, more precisely, by the peripheral ligand substitution patterns. A careful examination of the Mn^{III} coordination spheres of Mn12 structures indicates that whatever the positional isomer, the number of coordination sites substituted by carboxylates oxygen's is constant (i.e., 16 equatorial and 12 axial positions for the 8 Mn^{III} ions). When the acetates of the parent $[Mn_{12}(OAc)_{16}]$ cluster are replaced by the benzoate ligands, the crystal field around Mn^{III} ions is substantially modified. This is crucial for the d^4 Mn^{III} ions, showing a strong tendency toward JT distortion. Therefore, the substitution of acetates by ligands providing higher crystal field will globally stabilize the JT elongation along the main symmetry axis of the clusters. This is the case with these ligands, as it appears that the stabilization of the SR phase with respect to the FR depends also on the molecular symmetry and follows the trend $\mathbf{HL}_{3,4,5\text{-CB}} \geq \mathbf{HL}_{3,5\text{-CB}} \geq \mathbf{HL}_{4\text{-CB}} > \mathbf{HL}_{3,4\text{-CB}}$. Indeed, while for the three symmetrical systems, the SR magnetic phase remains predominant and the FR almost nonexistent, the relative abundance of the two phases is inverted in the nonsymmetrical $[Mn_{12}O_{12}(\mathbf{L}_{3,4\text{-CB}})_{16}(H_2O)_4]$ complex. Interestingly too, in the symmetrical systems, that is, with ligands $\mathbf{L}_{3,4,5\text{-CB}}$, $\mathbf{L}_{3,5\text{-CB}}$, $\mathbf{L}_{4\text{-CB}}$, this trend also is observed conjunctly with the decrease of the number of ether functions attached to the benzoate moieties coordinated to the Mn^{III} ions. As ether functions act as electron-donating groups, the electronic density of the aromatic ring is altered, and consequently the crystal field of the benzoate anchors is modified accordingly (vide supra, Supporting Information).

For the four complexes, the magnetization relaxation rate τ follows the Arrhenius equation (Figure 8). Only the parameters corresponding to the high-temperature peak (slow relaxing phase, SR) could be extracted with sufficient precision for each sample from the peak maxima of the χ'' versus T plots (Table 3). All fall within the expected ranges for Mn12 complexes: τ_0 lies in the interval of 5−10 ns; the effective energy barrier is comprised between 55 and 60 K.

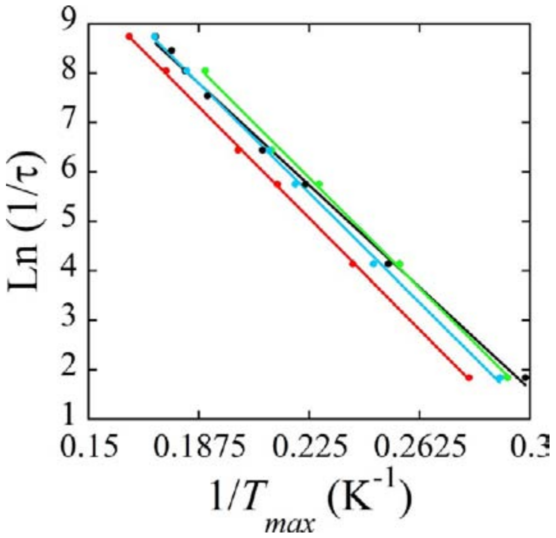

Figure 8. Plots of the natural logarithm of relaxation rate, ln(1/τ), versus inverse temperature for $[Mn_{12}O_{12}(\mathbf{L}_{3,4,5\text{-CB}})_{16}(H_2O)_4]$ (black), $[Mn_{12}O_{12}(\mathbf{L}_{3,5\text{-CB}})_{16}(H_2O)_4]$ (red), $[Mn_{12}O_{12}(\mathbf{L}_{3,4\text{-CB}})_{16}(H_2O)_4]$ (green), and $[Mn_{12}O_{12}(\mathbf{L}_{4\text{-CB}})_{16}(H_2O)_4]$ (cyan) using the χ'' versus T data for the SR species of Figure 7 and Table 3. Full lines correspond to the best fits obtained from an Arrhenius law (see text).

Finally, the shape of the magnetization versus field curves recorded at 1.8 K at about 700 G min^{-1} for the four hybridized compounds is typical for randomly oriented polycrystalline Mn12 species (Figure 9).[23] The magnetization curves exhibit an opened hysteresis loop characteristic of SMM behavior with a coercive field and a remnant magnetization (the absence of a saturation of the magnetization at high fields is due to the polycrystalline nature of the materials). The coercive field values at 1.8 K are in the range 0.13−0.6 T, in accordance with the relative proportion of the SR species versus the FR ones: the largest values (0.6−0.32 T) are indeed found for the derivatives having the largest SR species content (with respect to the FR one), whereas the smallest value (0.13 T) is obtained with the compound derived from $\mathbf{L}_{3,4\text{-CB}}$ ligand in which the JT distorted isomer (FR) is predominant. Moreover, one can discern that the variation of the measured values of the coercive field (and to some extend the remnant magnetization) for each sample seems also to be, at first sight, correlated to the ligand substitution pattern that is the number and position (symmetry) of mesogenic end-groups (Table 1): first the highest μ_0H_C value is found for the symmetrical systems (those having the highest SR/FR ratio), and second this value increases along the sequence $\mathbf{L}_{3,4\text{-CB}} < \mathbf{L}_{3,4,5\text{-CB}} < \mathbf{L}_{3,5\text{-CB}} \approx \mathbf{L}_{4\text{-CB}}$, that with ligand $L_{3,4\text{-CB}}$ giving rise to multiple regioisomers likely to contribute even more to the narrowing of the hysteresis loop at zero field.

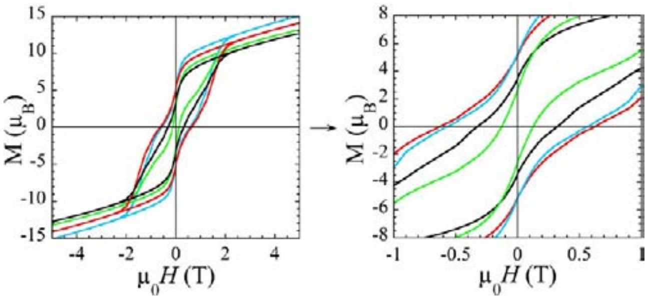

Figure 9. Magnetization versus applied field for $[Mn_{12}O_{12}(\mathbf{L}_{3,4\text{-CB}})_{16}(H_2O)_4]$ (green), $[Mn_{12}O_{12}(\mathbf{L}_{3,4,5\text{-CB}})_{16}(H_2O)_4]$ (black), $[Mn_{12}O_{12}(\mathbf{L}_{3,5\text{-CB}})_{16}(H_2O)_4]$ (red), and $[Mn_{12}O_{12}(\mathbf{L}_{4\text{-CB}})_{16}(H_2O)_4]$ (cyan) at 1.8 K (the right figure is a zoom of the central part of the figure on the left side).

■ DISCUSSION

All four Mn12 clusters have retained their original SMM magnetic behavior upon hybridization by structuring organic ligands, and the characteristic parameters are those expected for this archetypical mixed-valent cluster.[12] We noted however two subtle differences (recall that all measurements were performed under identical experimental conditions in all cases): (i) about the relative proportion of both SR and FR species, which appear to be correlated with the structure of the ligand (e.g., the symmetry of the substitution pattern), that is the overall symmetry of the complex and number of geometrical isomers, and (ii) concerning the large variations of the coercive field values (0.1−0.6 T), again correlated to the substitution pattern of the ligands, which affects the proximity of the clusters within the median plane of the smectic layers, on the one hand, and their relative out of plane orientation with respect to the layer normal, on the other hand, consequently to the pulling effect.

At this stage, it appeared thus pertinent to try finding trends or correlations between the magnetism of these LC hybridized Mn12 clusters and their arrangement within the mesophases. Obviously, this task is tricky, because events occurring at different temperatures (low-temperature magnetic properties versus room-temperature supramolecular organization) are compared. However, consequent to thermal annealing and rapid cooling, all mesomorphous clusters were analyzed under the same experimental conditions, once into their glassy smectic phase, which retains essentially the ordering and packing integrity of the mesophase. After the low-temperature magnetic measurements, the samples were removed from the sample holders, and analyzed by DSC and SAXS (from −50 to ca. 100 °C), revealing unmodified materials, and most importantly with the same thermal behaviors (identical DSC traces and glass transition temperatures) and supramolecular organizations (smectic mesophase) as before the experiments.

Primarily, the relative proportion between SR and FR species seems to be dependent on the substitution pattern of the ligands, as all of the symmetrical complexes exhibit a higher proportion of SR species than FR ones, while this ratio is inverted in the case of the nonsymmetrical complex (with 3,4-substitution). It is not surprising that the larger number of geometrical isomers generated by this complex would likely perturb the SR/FR ratio (vide supra). Secondary, another striking feature is the variation of the coercive field along the series, considering that the same experimental conditions were systematically reproduced for the measurements. From the above analyses, the two compounds that have the lowest coercivity are those whose cores are tilted out of the median plane of the smectic layers as deduced by SAXS and are the more compact systems (Figure 10), and it is not outrageously speculative to emphasize that the pulling or pressure effects of the peripheral mesogens (to reach the mesogenic outer sublayer) distort the cluster and affect its magnetic properties. Although the effect of the true nature of the 2D lattice symmetry (local in-plane arrangement of the clusters), which could not be unequivocally assigned (hexagonal versus square), on the magnetic properties could not be discriminated, an

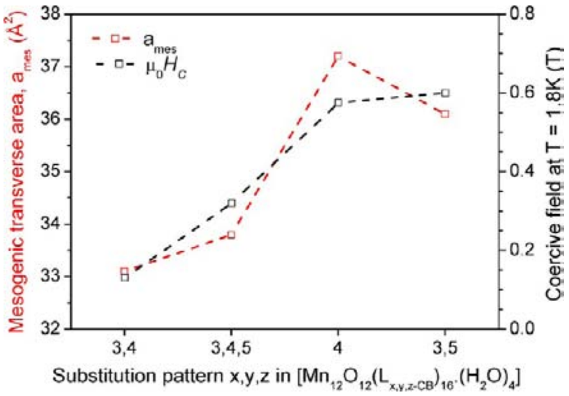

Figure 10. Evolution of the transverse molecular area, a_{mes}, and coercive field, $\mu_0 H_C$, as a function of the ligand-substitution patterns.

interesting observation however is that the further apart are the clusters, the smaller is the coercive field. It has been previously shown that intermolecular magnetic interactions were of outmost importance in the behavior of SMM, especially in the quantum tunneling of magnetization (QTM), which is indeed not purely molecular in origin.[52] The present work shows that it might be possible to finely tune the behavior of SMM, by allowing precise control of the intercluster distances (of the order of 20 Å) and their respective orientation.

■ CONCLUSION

In this study, we have reported on various SMM LC-hybridized clusters able to self-organize into a room-temperature smectic phase, which can be described by a bilayer structure made of outer mesogens sublayers with a short-range 2D in-plane arrangement of the clusters embedded in the median aliphatic sublayer. This study revealed that this molecular design, namely the grafting of mesogens around the Mn12 hard core, permitted subtle structural modifications without drastically transforming the mesophase organization (periodicity and compactness variations depending on the substitution pattern, enhanced thermal stability) and produced interesting new effects on the dynamic magnetic behavior (relative proportion of SR/FR species and coercive fields values), which may be considered for the design of future single molecule magnetic materials. All four Mn12 clusters have indeed retained their original SMM magnetic behavior upon hybridization by the structuring organic ligands, and the characteristic parameters expected for the this archetypical mixed-valent cluster could be finely tuned by the specific molecular design and supramolecular organization. To further develop these fundamental aspects and to optimize the various magnetic and mesomorphic properties, one will obviously have to design new LC Mn12, or to extend and adapt this strategy to other types of SMM clusters. For instance, taking advantage on the different reactivity of the equatorial and axial substituents,[53] potentially very interesting new molecular heterogeneous Mn12 hybrids bearing mixed (LC) ligands, with a high control of their distribution on both positions, showing uncommon supramolecular arrangements could be imagined. Concomitantly, many other fascinating and versatile molecular structures derived from mixed d−f complexes to high-nuclearity families of homo- and heterometallic based-materials could be sought and designed to form LC mesophases, appropriate mesogenic ligands being easily available, and emerge with unprecedented features, for example, higher temperature functioning being the most desirable one, essential for realistic technological applications. Last, still in view of the aforementioned development of a molecular magnetic memory, one may imagine its 3D implementation within such mesophases, taking profit of the original photosensitivity of Mn12 derivatives.[35] In addition to the density gain resulting from using bit elements much smaller than the current ones, one would also hugely benefit from going from 2D to 3D.

■ ASSOCIATED CONTENT

Ⓢ Supporting Information

Experimental section including techniques, syntheses of ligands and complexes, IR (Figures S1−S3) and ^{1}H NMR (Figures S4−S6) spectroscopies, DSC (Figures S7−S10, S22−S25) and TGA (Figure S21) curves, POM images (Figures S11−S20), XRD patterns (Figures S26−S28), molecular dynamics (Figures S29,S30), Jahn−Teller distortion diagrams in octahedral complexes (Figure S31), and tables (S1−S3). This material is available free of charge via the Internet at http://pubs.acs.org.

■ AUTHOR INFORMATION

Corresponding Author

bdonnio@ipcms.u-strasbg.fr

Present Address

[†]Department of Inorganic Chemistry, University of Geneva, 30 quai E. Ansermet, CH-1211 Geneva 4, Switzerland.

Notes

The authors declare no competing financial interest.

■ ACKNOWLEDGMENTS

This work was supported by the Swiss National Science Foundation (E.T.), the CNRS (J.-L.G., G.R., B.D.), and the Université de Strasbourg. We thank Dr. Cyril Bourgogne (MD) and Mr. Didier Burger (TGA).

■ REFERENCES

(1) Winpenny, R., Ed. Single-Molecule Magnets and Related Phenomena. *Structure and Bonding*; Springer: Berlin, 2006; Vol. *122*.

(2) Brooker, S.; Kitchen, J. A. *Dalton Trans.* **2009**, 7331−7340.

(3) (a) Leuenberger, M. N.; Loss, D. *Nature* **2001**, *410*, 789−793. (b) Cavallini, M.; Biscarini, F.; Gomez-Segura, J.; Ruiz, D.; Veciana, J. *Nano Lett.* **2003**, *3*, 1527−1530. (c) Wernsdorfer, W. *Nat. Mater.* **2007**, *6*, 174−176. (d) Bogani, L.; Wernsdorfer, W. *Nat. Mater.* **2008**, *7*, 179−186. (e) Stepanenko, D.; Trif, M.; Loss, D. *Inorg. Chim. Acta* **2008**, *361*, 3740−3745. (f) Winpenny, R. E. P. *Angew. Chem., Int. Ed.* **2008**, *47*, 7992−7994. (g) Wernsdorfer, W. *Int. J. Nanotechnol.* **2010**, *7*, 497−522.

(4) Vincent, R.; Klyatskaya, S.; Ruben, M.; Wernsdorfer, W.; Balestro, F. *Nature* **2012**, *488*, 357−360.

(5) (a) Gómez-Segura, J.; Veciana, J.; Ruiz-Molina, D. *Chem. Commun.* **2007**, 3699−3707. (b) Cavallini, M.; Facchini, M.; Albonetti, C.; Biscarini, F. *Phys. Chem. Chem. Phys.* **2008**, *10*, 784−793.

(6) Rogez, G.; Donnio, B.; Terazzi, E.; Gallani, J.-L.; Kappler, J.-P.; Bucher, J.-P.; Drillon, M. *Adv. Mater.* **2009**, *21*, 4323−4333.

(7) (a) Gatteschi, D.; Sessoli, R.; Cornia, A. *Chem. Commun.* **2000**, 725−732. (b) Winpenny, R. E. P. *J. Chem. Soc., Dalton Trans.* **2002**, 1−10. (c) Christou, G. *Polyhedron* **2005**, *24*, 2065−2075. (d) Brechin, E. K. *Chem. Commun.* **2005**, 5145−5153. (e) Aromi, G.; Brechin, E. K. *Struct. Bonding (Berlin, Ger.)* **2006**, *122*, 1−67. (f) Collison, D.; McInnes, E. J. L.; Brechin, E. K. *Eur. J. Inorg. Chem.* **2006**, 2725−2733. (g) Escuer, A.; Aromi, G. *Eur. J. Inorg. Chem.* **2006**, 4721−4736. (h) Evangelisti, M.; Luis, F.; De Jongh, L. J.; Affronte, M. *J. Mater. Chem.* **2006**, *16*, 2534−2549. (i) Bircher, R.; Chaboussant, G.; Dobe, C.; Güdel, H. U.; Ochsenbein, S. T.; Sieber, A.; Waldmann, O. *Adv. Funct. Mater.* **2006**, *16*, 209−220. (j) Roubeau, O.; Clérac, R. *Eur. J.*

Inorg. Chem. **2008**, 4325−4342. (k) Tasiopoulos, A. J.; Perlepes, S. P. *Dalton Trans.* **2008**, 5537−5555. (l) Atanasov, M.; Comba, P.; Hausberg, S.; Martin, B. *Coord. Chem. Rev.* **2009**, *253*, 2306−2314. (m) Kortz, U.; Müller, A. J.; van Slageren, J.; Schnack, N. S.; Dalal, M. D. *Coord. Chem. Rev.* **2009**, *253*, 2315−2327. (n) Murrie, M. *Chem. Soc. Rev.* **2010**, *39*, 1986−1995. (o) Kostakis, G. E.; Akoa, A.; Powell, A. K. *Chem. Soc. Rev.* **2010**, *39*, 2238−2271. (p) Sessoli, R.; Powell, A. K. *Coord. Chem. Rev.* **2010**, *253*, 2328−2341. (q) Kostakis, G. E.; Hewitt, I. J.; Ako, A. M.; Mereacre, V.; Powell, A. K. *Philos. Trans. R. Soc., A* **2010**, *368*, 1509−1536. (r) Wang, X.-Y.; Avendano, C.; Dunbar, K. R. *Chem. Soc. Rev.* **2011**, *40*, 3213−3238. (s) Inglis, R.; Milios, C. J.; Jones, L. F.; Piligkosd, S.; Brechin, E. K. *Chem. Commun.* **2012**, *48*, 181−190.

(8) Murugesu, M.; Habrych, M.; Wernsdorfer, W.; Abboud, K. A.; Christou, G. *J. Am. Chem. Soc.* **2004**, *126*, 4766−4767.

(9) Ako, A.; M. Hewitt, I. J.; Mereacre, V.; Clérac, R.; Wernsdorfer, W.; Anson, C. E.; Powell, A. K. *Angew. Chem., Int. Ed.* **2006**, *45*, 4926−4929.

(10) Lis, L. *Acta Crystallogr., Sect. B* **1980**, *36*, 2042−2046.

(11) (a) Sessoli, R.; Gatteschi, D.; Caneschi, A.; Novak, M. A. *Nature* **1993**, *365*, 141−143. (b) Sessoli, R.; Tsai, H.-L.; Schake, A. R.; Wang, S.; Vincent, J. B.; Folting, K.; Gatteschi, D.; Christou, G.; Hendrickson, D. N. *J. Am. Chem. Soc.* **1993**, *115*, 1804−1816.

(12) (a) Mertes, K. M.; Suzuki, Y.; Sarachik, M. P.; Myasoedov, Y.; Shtrikman, H.; Zeldov, E.; Rumberger, E. M.; Hendrickson, D. N.; Christou, G. *Solid State Commun.* **2003**, *127*, 131−139. (b) Bagai, R.; Christou, G. *Chem. Soc. Rev.* **2009**, *38*, 1011−1026.

(13) The $S = 10$ ground state is further split into 11 $\pm M_S$ sublevels (i.e., $2S + 1$) in zero field, and the $M_S = \pm 10$ levels are the lowest in energy.

(14) At the first order, $U_{\text{eff}} = S^2|D|$ or $(S^2 - 1/4)|D|$ for integer or half-integer spin-numbers, respectively.

(15) Paulsen, C.; Park, J.-G.; Barbara, B.; Sessoli, R.; Caneschi, A. *J. Magn. Magn. Mat.* **1995**, *140−144*, 379−380.

(16) Milios, C. J.; Vinslava, A.; Wernsdorfer, W.; Moggach, S.; Parsons, S.; Perlepes, S. P.; Christou, G.; Brechin, E. K. *J. Am. Chem. Soc.* **2007**, *129*, 2754−2755.

(17) Soler, M.; Wernsdorfer, W.; Sun, Z.; Ruiz, D.; Huffman, J. C.; Hendrickson, D. N.; Christou, G. *Polyhedron* **2003**, *22*, 1783−1788.

(18) Halcrow, M. A. *Chem. Soc. Rev.* **2013**, *42*, 1784−1795.

(19) When the symmetry of the metal complex is lowered from O_h to D_{4h} by elongation along the z axis, the original t_{2g} (d_{xy}, d_{xz}, and d_{yz}) and e_g (d_{z2} and d_{x2-y2}) levels (O_h symmetry) split into e_g (d_{xz} and d_{yz}), b_{2g} (d_{xy}), a_{1g} (d_{z2}), and b_{1g} (d_{x2-y2}) levels (D_{4h} symmetry) according to the character tables (Figure S31).

(20) Tasiopoulos, A. J.; Vinslava, A.; Wernsdorfer, W.; Abboud, K. A.; Christou, G. *Angew. Chem., Int. Ed.* **2004**, *43*, 2117−2121.

(21) (a) Przychodzeń, P.; Pełka, R.; Lewiński, K.; Supel, J.; Rams, M.; Tomala, K.; Sieklucka, B. *Inorg. Chem.* **2007**, *46*, 8924−8938. (b) Yang, C.-I.; Wernsdorfer, W.; Cheng, K.-H.; Nakano, M.; Lee, G.-H.; Tsai, H.-L. *Inorg. Chem.* **2008**, *47*, 10184−10186. (c) Kajiwara, T.; Nakano, M.; Takaishi, S.; Yamashita, M. *Inorg. Chem.* **2008**, *47*, 8604−8606. (d) Kajiwara, T.; Takahashi, K. I.; Hiraizumi, T.; Takaishi, S.; Yamashita, M. *Polyhedron* **2009**, *28*, 1860−1863. (e) Klöwer, F.; Lan, Y.; Nehrkorn, J.; Waldmann, O.; Anson, C. E.; Powell, A. K. *Chem.-Eur. J.* **2009**, *15*, 7413−7422. (f) Inglis, R.; Jones, L. F.; Karotsis, G.; Collins, A.; Parsons, S.; Perlepes, S. P.; Wernsdorfer, W.; Brechin, E. K. *Chem. Commun.* **2008**, 5924−5926.

(22) (a) Sieber, A.; Bircher, R.; Waldmann, O.; Carver, G.; Chaboussant, G.; Mutka, H.; Güdel, H.-U. *Angew. Chem., Int. Ed.* **2005**, *44*, 4239−4242. (b) Sanchez-Benitez, A. J.; Kamenev, K. V.; Moggach, S. A.; Lennie, A. R.; Warren, J. E.; Murrie, M.; Parsons, S.; Brechin, E. K. *Dalton Trans.* **2009**, 7390−7395. (c) Parois, P.; Moggach, S. A.; Sanchez-Benitez, J.; Kamenev, K. V.; Lennie, A. R.; Warren, J. E.; Brechin, E. K.; Parsons, S.; Murrie, M. *Chem. Commun.* **2010**, 1881−1883.

(23) Suzuki, Y.; Takeda, K.; Awaga, K. *Phys. Rev. B* **2003**, *67*, 132402.

(24) Boskovic, C.; Brechin, E. K.; Streib, W. E.; Folting, K.; Bollinger, J. C.; Hendrickson, D. N.; Christou, G. *J. Am. Chem. Soc.* **2002**, *124*, 3725−3736.

(25) Chakov, N. E.; Lee, S.-C.; Harter, A. G.; Kuhns, P. L.; Reyes, A. P.; Hill, S. O.; Dalal, N. S.; Wernsdorfer, W.; Abboud, K. A.; Christou, G. *J. Am. Chem. Soc.* **2006**, *128*, 6975−6989.

(26) Milios, C. J.; Inglis, R.; Bagai, R.; Wernsdorfer, W.; Collins, A.; Moggach, S.; Parsons, S.; Perlepes, S. P.; Christou, G.; Brechin, E. K. *Chem. Commun.* **2007**, 3476−3478.

(27) Cirera, J.; Ruiz, E.; Alvarez, S.; Neese, F.; Kortus, J. *Chem.-Eur. J.* **2009**, *15*, 4078−4087.

(28) Tuan, N. A.; Katayama, S.; Chi, D. H. *Phys. Chem. Chem. Phys.* **2009**, *11*, 717−729.

(29) *Handbook of Liquid Crystals*; Demus, D., Goodby, J. W., Gray, G. W., Spiess, H.-W., Vill, V., Eds.; Wiley-VCH: Weinheim, 1998.

(30) (a) Tschierske, C. *Annu. Rep. Prog. Chem., Sect. C: Phys. Chem.* **2001**, *97*, 191−267. (b) Binnemans, K.; Görller-Walrand, C. *Chem. Rev.* **2002**, *102*, 2303−2345. (c) Kato, T.; Mizoshita, N.; Kishimoto, K. *Angew. Chem., Int. Ed.* **2006**, *45*, 38−68. (d) Donnio, B.; Buathong, S.; Bury, I.; Guillon, D. *Chem. Soc. Rev.* **2007**, *36*, 1495−1513. (e) Tschierske, C. *Chem. Soc. Rev.* **2007**, *36*, 1930−1970. (f) Goodby, J. W.; Saez, I. M.; Cowling, S. J.; Görtz, V.; Draper, M.; Hall, A. W.; Sia, S.; Cosquer, G.; Lee, S.-E.; Raynes, E. P. *Angew. Chem., Int. Ed.* **2008**, *47*, 2754−2787. (g) Bruce, D. W. *Struct. Bonding (Berlin)* **2008**, *126*, 161−180. (h) Bisoyi, H. K.; Kumar, S. *Chem. Soc. Rev.* **2011**, *40*, 306−319. (i) Tschierske, C. *Top. Curr. Chem.* **2012**, *318*, 1−108.

(31) (a) Kumar, S. *Chem. Soc. Rev.* **2006**, *35*, 83−109. (b) Laschat, S.; Baro, A.; Steinke, N.; Giesselmann, F.; Hägele, C.; Scalia, G.; Judele, R.; Kapatsina, E.; Sauer, S.; Schreivogel, A.; Tosoni, M. *Angew. Chem., Int. Ed.* **2007**, *46*, 4832−4887. (c) Sergeyev, S.; Pisula, W.; Geerts, Y. H. *Chem. Soc. Rev.* **2007**, *36*, 1902−1929. (d) Kumar, S. *Liq. Cryst.* **2009**, *36*, 607−638. (e) Pisula, W.; Zorn, M.; Young, J. C.; Müllen, K.; Zentel, R. *Macromol. Rapid Commun.* **2009**, *30*, 1179−1202. (f) Kaafarani, B. R. *Chem. Mater.* **2011**, *23*, 378−396.

(32) Terazzi, E.; Bourgogne, C.; Welter, R.; Gallani, J.-L.; Guillon, D.; Rogez, G.; Donnio, B. *Angew. Chem., Int. Ed.* **2008**, *47*, 490−495.

(33) Grumbach, N.; Barla, A.; Joly, L.; Donnio, B.; Rogez, G.; Terazzi, E.; Kappler, J.-P.; Gallani, J.-L. *Eur. Phys. J. B* **2010**, *73*, 103−108.

(34) Donnio, B.; Rivière, E.; Terazzi, E.; Voirin, E.; Aronica, C.; Chastanet, G.; Luneau, D.; Rogez, G.; Scheurer, F.; Joly, L.; Kappler, J.-P.; Gallani, J.-L. *Solid State Sci.* **2010**, *12*, 1307−1313.

(35) Rivière, E.; Donnio, B.; Voirin, E.; Rogez, G.; Kappler, J.-P.; Gallani, J.-L. *J. Mater. Chem.* **2010**, *20*, 7165−7168.

(36) Chuard, T.; Deschenaux, R.; Hirsch, A.; Schönberger, H. *Chem. Commun.* **1999**, 2103−2104.

(37) (a) Felder-Flesch, D.; Rupnicki, L.; Bourgogne, C.; Donnio, B.; Guillon, D. *J. Mater. Chem.* **2006**, *16*, 304−309. (b) Campidelli, S.; Brandmüller, T.; Hirsch, A.; Saez, I. M.; Goodby, J. W.; Deschenaux, R. *Chem. Commun.* **2006**, 4282−4284. (c) Gottis, S.; Kopp, C.; Allard, E.; Deschenaux, R. *Helv. Chim. Acta* **2007**, *90*, 957−962.

(38) Terazzi, E.; Jensen, T. B.; Donnio, B.; Buchwalder, K.; Bourgogne, C.; Rogez, G.; Heinrich, B.; Gallani, J.-L.; Piguet, C. *Dalton Trans.* **2011**, *40*, 12028−12032.

(39) Li, C.-Z.; Matsuo, Y.; Nakamura, E. *J. Am. Chem. Soc.* **2009**, *131*, 17058−17059.

(40) Molard, Y.; Dorson, F.; Cîrcu, V.; Roisnel, T.; Artzner, F.; Cordier, S. *Angew. Chem., Int. Ed.* **2010**, *49*, 3351−3353.

(41) (a) Li, W.; Yi, S.; Wu, Y.; Wu, L. *J. Phys. Chem. B* **2006**, *110*, 16961−16966. (b) Yin, S.; Li, W.; Wang, J.; Wu, L. *J. Phys. Chem. B* **2008**, *112*, 3983−3988. (c) Li, W.; Yin, S.; Wang, J.; Wu, L. *Chem. Mater.* **2008**, *20*, 514−522. (d) Zhang, T.; Liu, S.; Kurth, D. G.; Faul, C. F. J. *Adv. Funct. Mater.* **2009**, *19*, 642−652. (e) Yang, Y.; Wang, Y.; Li, H.; Li, W.; Wu, L. *Chem.-Eur. J.* **2010**, *16*, 8062−8071. (f) Floquet, S.; Terazzi, E.; Hijazi, A.; Guénée, L.; Piguet, C.; Cadot, E. *New J. Chem.* **2012**, *36*, 865−868.

(42) (a) Nealon, G. L.; Greget, R.; Dominguez, C.; Nagy, Z. T.; Guillon, D.; Gallani, J. L.; Donnio, B. *Beilstein J. Org. Chem.* **2012**, *8*,

349−370. (b) Stamatoiu, O.; Mirzaei, J.; Feng, X.; Hegmann, T. *Top. Curr. Chem.* **2012**, *318*, 331−394.

(43) (a) Kouwer, P. H. J.; Mehl, G. H. *J. Am. Chem. Soc.* **2003**, *125*, 11172−11173. (b) Kouwer, P. H. J.; Pourzand, J.; Mehl, G. H. *Chem. Commun.* **2004**, 66−67. (c) Cardinaels, T.; Driesen, K.; Parac-Vogt, T. N.; Heinrich, B.; Bourgogne, C.; Guillon, D.; Donnio, B.; Binnemans, K. *Chem. Mater.* **2005**, *17*, 6589−6598.

(44) (a) Donnio, B.; Guillon, D. *Adv. Polym. Sci.* **2006**, *201*, 45−155. (b) Saez, I. M.; Goodby, J. W. *Struct. Bonding (Berlin, Ger.)* **2008**, *128*, 1−62. (c) Imrie, C. T.; Henderson, P. A.; Yeap, G.-Y. *Liq. Cryst.* **2009**, *36*, 755−777.

(45) For $[\mathrm{Mn}_{12}\mathrm{O}_{12}(\mathbf{L}_{3,4,5}\text{-CB})_{16}(\mathrm{H}_2\mathrm{O})_4]$ at lower temperature, this diffuse scattering is reversibly transformed and substantially sharpened (the peak position is also slightly shifted to lower angles).

(46) Bourgogne, C.; Bury, I.; Gehringer, L.; Zelcer, A.; Cukiernik, F.; Terazzi, E.; Donnio, B.; Guillon, D. Molecular Dynamics simulations of liquid crystalline dendritic architectures. In *Atomic-Scale Modeling of Nanosystems and Nanostructured Materials*; Massobrio, C., Bulou, H., Goyhenex, Ch., Eds.; *Lecture Notes in Physics*; Springer: Berlin-Heidelberg, Germany, 2010; Vol. *795*, pp 103−128.

(47) Gatteschi, D.; Sessoli, R. *Angew. Chem., Int. Ed.* **2003**, *42*, 268−297.

(48) (a) Takeda, K.; Awaga, K.; Inabe, T. *Phys. Rev. B* **1998**, *57*, R11062. (b) An, J.; Chen, Z.-D.; Bian, J.; Chen, J.-T.; Wang, S.-X.; Gao, S.; Xu, G.-X. *Inorg. Chim. Acta* **2000**, *299*, 28−34. (c) Aubin, S. M. J.; Sun, Z.; Eppley, H. J.; Rumberger, E. M.; Guzei, I. A.; Folting, K.; Gantzel, P. K.; Rheingold, A. L.; Christou, G.; Hendrickson, D. N. *Inorg. Chem.* **2001**, *40*, 2127−2146.

(49) (a) Takeda, K.; Awaga, K. *Phys. Rev. B* **1997**, *56*, 14560−14565. (b) Ruiz-Molina, D.; Gerbier, P.; Rumberger, E.; Amabilino, D. B.; Guzei, I. A.; Folting, K.; Huffman, J. C.; Rheingold, A.; Christou, G.; Veciana, J.; Hendrickson, D. N. *J. Mater. Chem.* **2002**, *12*, 1152−1161. (c) Awaga, K.; Suzuki, Y.; Hachisuka, H.; Takeda, K. *J. Mater. Chem.* **2006**, *16*, 2516−2521.

(50) (a) Ruiz, D.; Sun, Z.; Albela, B.; Folting, K.; Ribas, J.; Christou, G.; Hendrickson, D. N. *Angew. Chem., Int. Ed.* **1998**, *37*, 300−302. (b) Zhao, H.; Berlinguette, C. P.; Bacsa, J.; Prosvirin, A. V.; Bera, J.; Tichy, K.; Schelter, S. E.; Dunbar, E. J. K. R. *Inorg. Chem.* **2004**, *43*, 1359−1369. (c) Eppley, H. J.; Tsai, H.; Vries, N.; Folting, K.; Christou, G.; Hendrickson, D. N. *J. Am. Chem. Soc.* **1995**, *117*, 301−317. (d) Aubin, M. J.; Sun, Z. M.; Eppley, H. J.; Rumberger, R. M.; Guzei, I. A.; Folting, K.; Gantzel, P. K.; Rheingold, A. L.; Christou, G.; Hendrickson, D. N. *Polyhedron* **2001**, *20*, 1139−1145. (e) Coronado, E.; Forment-Aliaga, A.; Gaita-Ariño, A.; Giminéz-Saiz, C.; Romero, F. M.; Wernsdorfer, W. *Angew. Chem., Int. Ed.* **2004**, *43*, 6152−6156. (f) Ruiz-Molina, D.; Mas-Torrent, M.; Gomez, J.; Balana, A. I.; Domingo, N.; Tejada, J.; Martinez, M. T.; Rovira, C.; Veciana. *J. Adv. Mater.* **2003**, *15*, 42−45.

(51) Four positional isomers have been described in the literature: 1:1:1:1 (S_4 symmetry), 2:0:2:0 (D_2 symmetry), 1:2:1, and 1:1:2 (the notation indicates the number of water molecules coordinated to type II $\mathrm{Mn}^{\mathrm{III}}$ ions).

(52) (a) Wernsdorfer, W.; Ohm, T.; Sangregorio, C.; Sessoli, R.; Gatteschi, D.; Paulsen, C. *Physica B* **2000**, *284*, 1229−1230. (b) Wernsdorfer, W.; Bhaduri, S.; Tiron, R.; Hendrickson, D. N.; Christou, G. *Phys. Rev. Lett.* **2002**, *89*, 197201. (c) Wernsdorfer, W.; Allaga-Alcalde, N.; Hendrickson, D. N.; Christou, G. *Nature* **2002**, *416*, 406−409.

(53) Artus, P.; Boskovic, C.; Yoo, J.; Streib, W. E.; Brunel, L.-C.; Hendrickson, D. N.; Christou, G. *Inorg. Chem.* **2001**, *40*, 4199−4210.